[Frontiers in Bioscience S3, 1308-1331, June 1, 2011]

Electrochemical and optical biosensors based on nanomaterials and nanostructures: A Review

Ming Li[1], Rui Li[1,2], Chang Ming Li[2] and Nianqiang Wu[1]

[1]Department of Mechanical and Aerospace Engineering, WVNano Initiative, West Virginia University, Morgantown, WV 26506-6106, USA; [2]School of Chemical and Biomedical Engineering, Nanyang Technological University, 70 Nanyang Drive, Singapore 637457, Singapore

TABLE OF CONTENTS

1. ABSTRACT

Nanomaterials and nanostructures exhibit unique size-tunable and shape-dependent physicochemical properties that are different from those of bulk materials. Advances of nanomaterials and nanostructures open a new door to develop various novel biosensors. The present work has reviewed the recent progress in electrochemical, surface plasmon resonance (SPR), surface-enhanced Raman scattering (SERS) and fluorescent biosensors based on nanomaterials and nanostructures. An emphasis is put on the research that demonstrates how the performance of biosensors such as the limit of detection, sensitivity and selectivity is improved by the use of nanomaterials and nanostructures.

2. INTRODUCTION

Over the last two decades, the booming of nanotechnology, especially the exponential growth in the design and synthesis of nanostructured materials at dimensions between approximately 1 and 100 nm, has infused new vigor into the development of novel sensing systems and enhancement of the performance of the bioanalytical assays (1). The size of nanomaterials (Figure 1) is comparable to the dimensions of typical biomolecule recognition probes in biosensors and to those of the biological analytes as well (2,3-5). The recent development of synthetic chemistry has made it possible to produce high-quality nanomaterials, including nanoparticles (nanospheres, nanorods, nanowires and nanotubes),

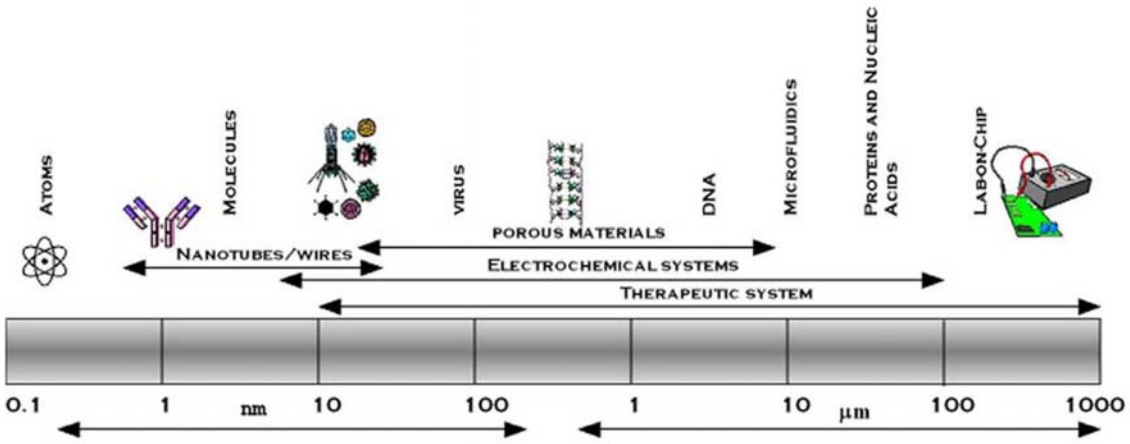

Figure 1. Size and compatibility. Reproduced with permission from (2).

nanoarrays and their composites (6,7). These nanostructured materials have been extensively used to fabricate biosensors due to their significant advantages over micro-scale and bulk materials (8-17), including: (i) large specific surface-volume ratio, (ii) significant size-tunable properties, (iii) shape-dependent properties, (iv) reduced energy consumption, (v) miniaturized size of sensors, and *etc*.

To date, nanomaterial-based biosensors utilize the sensitive response of the optical or the electronic properties of nanomaterials to biomolecular binding events. That is, the sensing signal is collected by the change in the intensity or the peak position of optical absorption, reflection, fluorescence emission, surface plasmon resonance (SPR), surface-enhanced Raman scattering (SERS) and electrochemical potential/current under various environments. Accordingly, fluorescent, SPR, SERS and electrochemical biosensors have been developed. The publications in this area exceed 400 papers per year according to the statistics from the Web of Science®. Several reviews have contributed to the synthetic methodology of nanomaterials and the development of optical and electrochemical biosensors (18-23). Herein, this paper will highlight the progress in the applications of nanomaterials and nanostructures in optical and electrochemical biosensors. In particular, the correlation of nanostructures with the performance of biosensors will be addressed.

3. ELECTROCHEMICAL BIOSENSORS

3.1. The beauty of nanomaterials in electrochemical biosensors

The proper interfacing of biological recognition events with electric signal transduction is indispensable for the construction of electrochemical biosensors. Nanomaterials can provide excellent solutions to meet biointerfacing requirements, owing to their tailorable physical and chemical properties by varying size, composition and shape at the nanoscale (24,25). Nanomaterials are employed as either electrodes (2) or as modification agents for electrodes (26). They offer a large specific active surface area for biomolecule immobilization and facilitate the electron transfer between the solid surface and the biomolecules, leading to high sensitivity as well as a low detection limit for electrochemical biosensors. For example, application of nanomaterials in a microorganism sensor leads to the detection limit as low as 1 colony forming units (CFU)/mL while that of the conventional biosensors is between 10^3 and 10^4 CFU/mL (2). A high-temperature CO electrochemical sensor utilizing porous CuO-ZnO nanocomposite as the sensing electrode exhibited high sensitivity toward CO as low as 25 ppm in air at 500 °C, because the highly porous structure of the nanocomposite successfully increased the loading capacity of the electrode (27). An amperometric glucose sensor in which ZnO nanowires were used to immobilize glucose oxidase (GOx) has exhibited a detection limit of 0.7 µM at signal/noise=3 (28), which is 10 folds lower than that (70 µM) of the reported glucose sensor based on titanium dioxide sol-gel matrix (29).

Selectivity toward a specific analyte is crucial to biosensors, especially in the early diagnostic applications. High selectivity could be achieved via using nanomaterials or nanostructures to modify the electrode or to directly act as the nanoelectrode (1,30). For enzymatic electrochemical biosensors, it is difficult for electrons to transfer directly between the conventional electrode surface and the redox active center deeply embedded in the insulated protein shells. For instance, the depth of the redox center for GOx is about 13 Å, leading to a slow electron transfer rate between the active site of GOx and the electrode surface (31). Nanomaterials can promote the electron transfer from the redox active center to the electrode surface, which thus makes it possible for the substrate oxidation to occur at a lower potential. This avoids the generation of noise by electro-active interferences that co-exist with the analyte of interest. A typical example is the electrode modified by the Pt nanowire/carbon nanotube (CNT)/chitosan nanocomposite film. It could detect glucose at a low oxidation potential, which could overcome the interferences from electro-active species usually present in

physiological samples such as ascorbic acid (AA) and uric acid (UA). As a result, high selectivity and good specificity have been achieved with the biosensor (32).

The response time has also been proved to be reduced by using nanomaterials in an electrode to accelerate electron transfer. A biosensor with the electrode modified by copper nanoparticle (NP)/CNT composite showed only 10 s of response time to glucose (33). In addition, a glucose biosensor in which the Au electrode was modified by six bilayers of GOx/Au NPs exhibited a response time of less than 4 s (34).

In the following sections, advantages of the nanomaterial/nanostructrure application in electrochemical biosensors are reviewed in three prominent aspects: immobilization of the biomolecules, enhancement of the mass transport and promotion of the electron transfer.

3.2. Immobilization of biomolecules

In electrochemical biosensors, immobilization of molecular recognition probes is a key step to keep the bioacitivity as well as to control the orientation and conformation of biomolecules. The degree of retaining biomolecules in their active forms will directly affect both the stability and the reproducibility of biosensor (35). Proteins (e.g., enzymes) directly adsorbed on a bare (unmodified) electrode like carbon, platinum or gold are inclined to denature, leading to fouling of electrodes (36). Thus, a polymer matrix or a covalent attachment on functional groups was usually employed as the entrapment agent (30). The emergence of nanomaterials has endowed electrochemical biosensing alternative ways for immobilization of biomolecule recognition probes. Nanomaterials possess a high surface-to-volume ratio and the three-dimensional (3-D) network assembled by one-dimensional (1-D) nanostructures exhibits a porous structure in which individual 1-D nanostructures remain a large area of active surface. Such architectures are effective in alleviating surface fouling effects, leading to the enhanced retention of bioactivity. As a result, a large amount of biological molecules (e.g., enzyme, antibody, cell, and DNA) can be immobilized on the active surface of nanomaterials, thus giving an intense response signal (30).

3.2.1. Direct adsorption

Titanium dioxides are known to be environmentally benign, chemically stable in physiological fluids, and have good mechanical strength. The titanate surface contains functional hydroxyl groups that offered a hydrophilic surface. The hydrophilic surfaces are expected to provide an aqueous-like environment that facilitates the stabilization of the immobilized proteins (37). It has been reported that adsorbed proteins on nanocrystalline TiO_2 surfaces exhibited less denaturation (38). Wu's group has employed the titanate nanotubes (TNTs) to develop a reagentless electrochemical biosensor for lactate detection (36). The results demonstrated that the nanotubes formed a porous 3-D network as the enzyme support matrix. Negatively charged groups usually present on the TNT surface at the working PBS solution could favor the enzyme adsorption, which results from the electrostatic interactions between the negatively charged groups on the TNT surface and the positively charged surface lysine and arginine residues of lactate oxidase (LOx). A large amount of enzyme can be loaded onto the electrode due to the large specific surface area of individual TNTs and the unique porous 3-D network. Additionally, this architecture provides a friendly micro-environment for immobilization of enzymes, which could retain the biocatalytic activity of enzymes. Cyclic voltammetry and amperometry tests revealed that the LOx enzyme supported on the TNTs maintained their substrate-specific catalytic activity, which directly resulted in the excellent performance of the biosensor with a sensitivity of 0.24 $\mu A\ cm^{-2}\ mM^{-1}$, a 90% response time of 5 s, and a linear response in the range from 0.5 to 14 mM.

3.2.2. Covalent binding

An alternative way to avoid the instability and inactivation of biomolecules is to covalently bind proteins to the NP surfaces (39). Low-molecular bifunctional linkers, which have the anchor groups for their attachment to NP surfaces and the functional groups for their covalent coupling to the target biomolecules, have been extensively used in the generation of covalent-tethered conjugates of biomolecules with various NPs (40). Anchor groups such as thiols, disulfides, or phosphine ligands are often used for the binding of the bifunctional linkers to Au, Ag, CdS, and CdSe NPs (41). Various terminal functional groups such as amine, active ester and maleimide groups are commonly used to covalently couple biological compounds by means of carbodiimide-mediated esterification and amidation reactions or through reactions with thiol groups (40).

In fabrication of an amperometric immunosensor based on gold NPs (GNPs)/CNTs hybrid platform, covalent binding was employed to immobilize biological receptors. As shown in Figure 2, both the immobilization of Ab_1 onto the GNP-modified glassy carbon electrode (GCE) and the connection of Ab_2 to HRP-GNPs were achieved by the strong interaction between GNPs and the mercapto or the primary amine groups in biomolecules. The GNP/CNT nano-hybrids were covered on the surface of a GCE to form an effective antibody immobilization matrix. This rendered the immobilized biomolecules with the high stability, the well-preserved bioactivity and the uniform orientation due to the specific combination in covalent binding. The cyclic voltammetric behavior of the immunosensor has demonstrated that the oxidation of OPD by H_2O_2 went to completion quickly by catalysis of HRP. The resulting electrochemical immunosensor exhibited a linear response range between 0.125 and 80 ng/mL with a detection limit of 40 pg/mL IgG (43).

3.2.3. Layer-by-layer assembly

The layer-by-layer (LbL) assembly technique is based on the alternating adsorption of oppositely charged cationic and anionic species (44). Because both of them bear surface charges, it is feasible to conjugate nanomaterials with biomolecules via the LbL assembly technique onto the electrode surface for electrochemical applications (45). Lee and co-workers have prepared an ion-sensitive conductometric glucose sensor by LbL

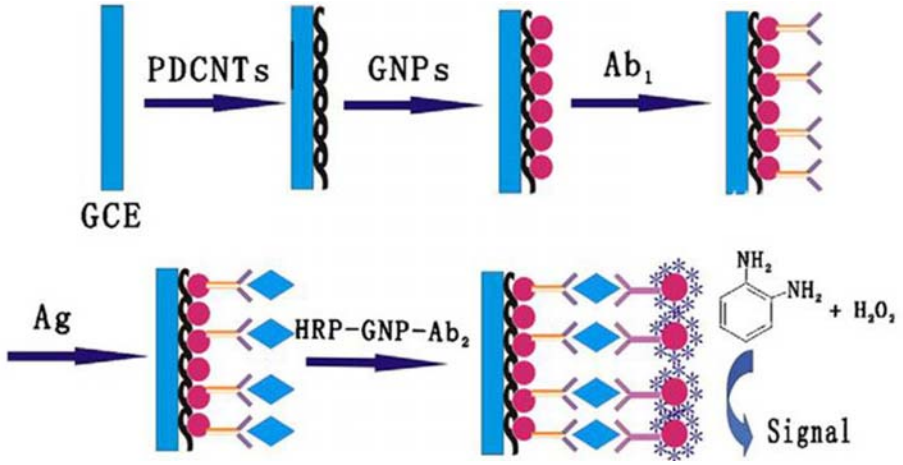

Figure 2. The immunoassay procedure of GNPs/PDCNTs modified immunosensor using horseradish peroxidase-Gold NPs-antibody$_2$ (HRP-GNPs-Ab$_2$) conjugates as label. Reproduced with permission from (42).

assembling of single-walled carbon nanotube (SWNT) and enzyme GOx (46). The carboxylated SWNT and negatively-charged GOx were self-assembled alternatively with a positively charged polyelectrolyte, poly (diallyldimethylammonium chloride, PDDA). The SWNT multilayer showed the pH-dependent conductance, which exponentially decreased with the pH increase. The concentration of glucose was measured based on the fact that protons from glucose oxidation catalyzed by GOx could change the local pH in the vicinity of SWNT multilayer, thereby modulating the conductance. The overall sensitivity was 10.8 μA/mM and the detection limit of the biosensor was 1 pM at the bias voltage of 0.6 V. The results indicated that the LbL assembled SWNT/PDDA/GOx multilayer effectively retained the bioactivity and controlled the conformation of the GOx.

3.3. Enhancement of the mass transport

In electrochemical biosensors, modification of the electrode with nanomaterials helps shorten the diffusion pathway. As the electrode size decreases, radial diffusion becomes dominant in electrochemical reactions (47), thus the mass transport rate increases, leading to the reduction of response time. In other words, mass transport increases with decrease in the electrode size (48), which is another advantage offered by nanomaterials used in electrochemical biosensors (30).

Superparamagnetic Fe_3O_4 NPs functionalized with dimercaptosuccinic acid (DMSA) were employed to develop a field-deployable electrochemical sensor for directly monitoring the toxic metals in urine (49). The authors declared that the mass transport of heavy metals to the sensor surface was boosted by the Fe_3O_4 NPs due to their small size. As a result, the sensor could detect 0.5 ppb Pb, and yielded a linear response from 0 to 50 ppb of Pb and excellent reproducibility.

Nanoelectrodes are able to enhance the mass transport and to improve the faradic to charging current ratio, leading to a low noise and high sensitivity (30). Another exciting virtue of nanoelectrodes for biological detection is that the active regions of nanoelectrodes allow packing a huge number of sensing elements onto a small given footprint of a device in which individual sensing elements are poised at different potentials, coated with different layers or even located within different regions of sample matrix (30). Individual nanoscale electrodes have some disadvantage such as extremely small current to be achieved. Thus, there is an incentive to develop nanoelectrode arrays (NEAs) or nanoelectrode ensembles (NEEs). Different from the linear diffusion feature of the mass transport in conventional macroelectrodes (Figure 3a), it is found that, as the size of individual electrodes in a NEA decreases while the pitch of individual electrodes increases, the diffusion layers at individual electrodes become independent of each other. In this case, the current response is dominated by the 3-D radial diffusion around individual nanoelectrodes (Figure 3c), especially when the scan rate is relatively fast. Consequently, a sigmoid-shaped voltammogram will occur (Figure 3c). The total Faradic current of the NEA is the sum of the current values of individual nanoelectrodes in the NEA. However, if the separation is insufficiently large and the scan rate is very low, the radial diffusion boundary layers totally overlap with each other (Figure 3b). As a result, a single diffusion layer covers the whole geometric area of the nanoelectrode array, thus a conventional peak-shaped voltammogram will occur. In this case, the total Faradic current is proportional to the geometric area of the electrode array.

Generally, the mass transport of reactants to the electrode surface is more sluggish than the electron transfer in electrochemical reactions. It is difficult to measure an electron transfer rate. By applying a NEA, a high rate of mass transport at individual nanoelectrodes enables the measurement of fast electrochemical reactions (47). Since most NEE fabrication methods have limited flexibility in controlling the size and shape of individual electrodes, the resulted random distribution of individual electrodes in a NEE makes it difficult to prevent the overlap of the mass diffusion layer. Hence, more efforts have been focused on

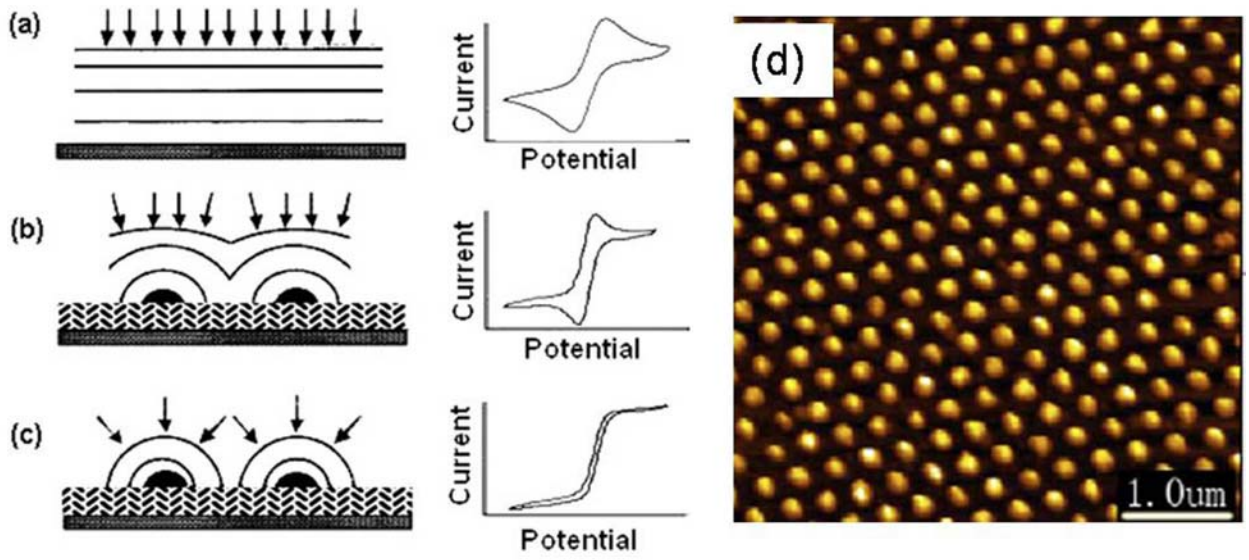

Figure 3. Schematic illustration of different diffusion fields induced by different electrode architectures and scan rates: (a) linear diffusion on a macroelectrode; (b) overlapped radial diffusion on a nanoelectrode array; (c) independent radial diffusion around individual nanoelectrodes in a NEA; (d) 3D AFM image of nanoelectrode array. Reproduced with permission from (50).

the development of long-range-ordered NEAs with controlled electrode size and spacing (pitch) (50). Wu and co-workers have demonstrated a novel NEA in which the gold hemispheres act as individual electrodes that are separated with an insulating polypyrrole (PPY) film as shown in Figure 3 (d) (50). They found that the cyclic voltammetry measurement of the NEA showed a sigmoid-shaped voltammogram, which is the electrochemical characteristic of a NEA. The created large-area, high-quality nanostructure array patterns will pave the way for the fabrication of low-cost, high-throughput and high-resolution electrochemical bioanalysing platform.

3.4. Promotion of the electron transfer

As discussed in Section 3.1, the redox active center is insulated by the protein matrix for most enzymes, preventing direct electron transfer to the electrode. Thus, the establishment of effective electron transfer between the active center of the biomolecule recognition probe and the electrode is critical for the development of electrochemical biosensors (1,30). Generally, it requires a relatively high oxidation potential for the direct amperometric detection to operate on a bare electrode (50). With such a high potential applied, however, common interferences arising from the oxidation of electroactive species such as AA and UA (51) cannot be avoided so that it will be difficult to identify the signal generated by the substrate of interest. It is known that electron transfer between the electrode and the redox center of enzyme could be promoted when some nanostructured materials are employed to modify the electrode (36), which will render a biosensor with enhanced current response at a low operating potential, and thus prohibit undesired interference. In the enhancement of the electron transfer in electrochemical biosensors, nanomaterials can act in the following ways.

3.4.1. Electron mediators/shuttles

Crumbliss and co-workers have prepared enzymatic sensors by modification of GCEs with the enzyme-gold nanoparticles (Au NPs) for detection of H_2O_2 (52,53) and glucose (52). Enzymes were first adsorbed on the colloidal gold and then the sol-containing the mixture was electrodeposited onto the GCEs. Au NPs also worked as electron mediators between the prosthetic groups of the enzymes and the electrode surface, and therefore facilitate the electron transfer process.

Wu and co-workers (36) have developed an electrochemical biosensor for lactate detection by the immobilization of LOx enzyme on the 3-D porous TNT network. By comparison of the cyclic voltammograms, it was found that the oxidation peak current of the Au-Nafion®-TNTs-LOx electrode was about 13 times higher than that of the Au-Nafion®-LOx electrode without TNTs. The author proposed that the nanotubes acted as effective shuttles for the electron transfer from the active redox co-factor (FAD/FADH2) of LOx to the gold electrode, successfully obviating the general need of redox mediators for electrochemical enzymatic sensors. A possible mechanism of the direct electron transfer here could be proposed according to the hypothesis by Guiseppi-Elie et al (54), in which an enzyme supported on a nanotube is analogous to a balloon sitting on a sharp needle, and individual nanotubes could penetrate into the protein shell of the flavoenzymes, thus are physically contacted with or located within the electron tunneling distance of the FAD prosthetic group of the enzyme due to the small diameter of the nanotubes.

3.4.2. Direct wiring

Controlled assembly/alignment and proper functionalization of nanostructure is an essential step prior

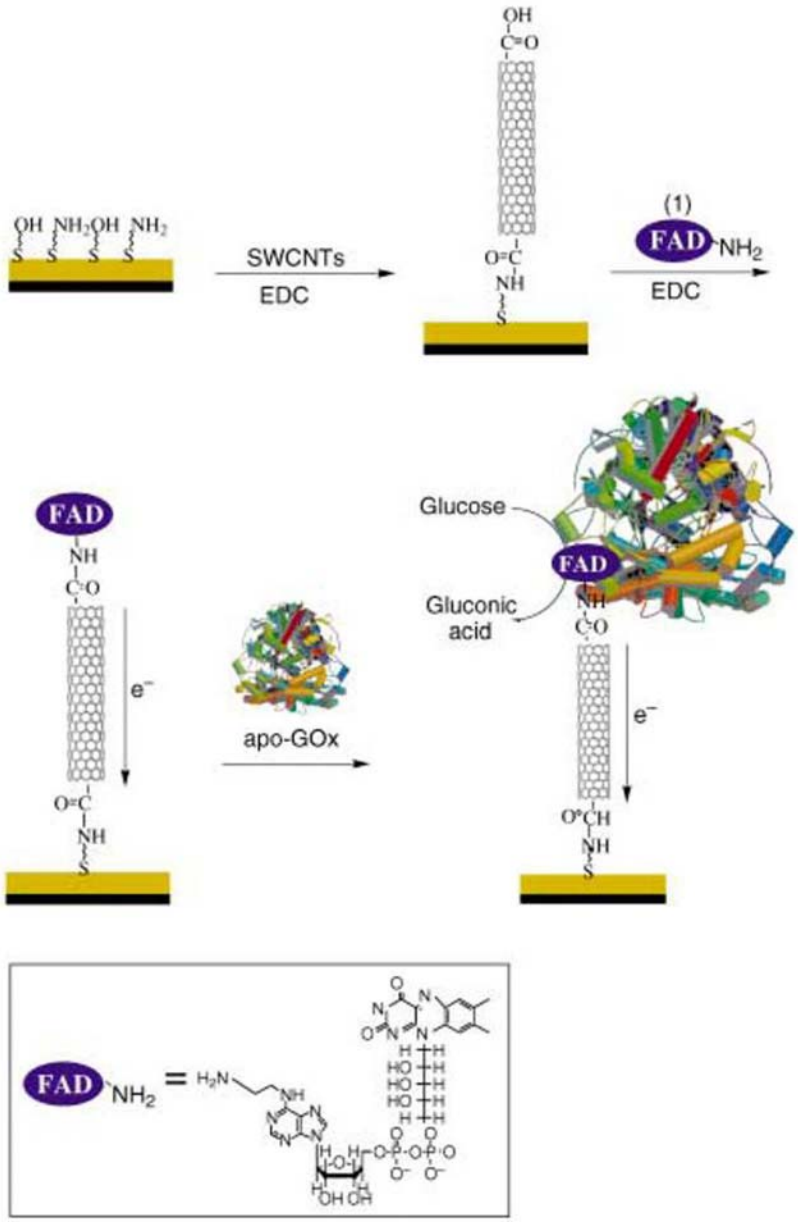

Figure 4. Assembly of the SWCNT electrically contacted glucose oxidase electrode. Reproduced with permission from (55).

to immobilization of enzymes. If nanomaterials are properly functionalized and aligned well, they can even act as molecular wires to allow direct electron transfer from the redox protein to the electrode (30). Willner group (55) has demonstrated the functionalization of the vertically aligned SWNTs (Figure 4). The GOx enzyme was reconstituted at the immobilized flavin adenine dinucleotide (FAD), which was covalently attached to the functionalized SWNT end. The aligned SWNTs acted as the molecular wires to allow direct electron transfer between the redox center of biomolecules and the underlying electrode surface. Thus, this is extremely attractive for construction of a reagentless biosensor, which is desirable for real-time monitoring during biochemical tests.

Willner and co-workers have also developed a system by reconstitution of apo-GOx molecules on individual Au NP-FAD units. A metallic NP with the proper dimensions and functionalization adjacent to the redox center of enzyme acted as a current collector and as an electron relay to a macroelectrode (56). Cyclic voltammograms of the electrode with the apo-GOx showed that the glucose electrooxidation current increased with the glucose concentration up to the value of 1.2×10^{-2} M, which was twice the Michaelis constant of the native enzyme. The result revealed that the Au NPs acted as an electron relay or "electrical nanoplug" for the alignment of the enzyme on the conductive support and for the electrical wiring of its redox-active center, and thus led to the transcendence in the

electron transfer features of the reconstituted GOx over the native enzyme.

3.4.3. Single nanoelectrode

It is difficult to detect ultra-low concentration of molecules due to small signal and the large background current associated with stray capacitance and impurities (2). The electrode size is thus reduced to minimize the background current. When the size of electrodes is decreased to the nanometer scale, many changes will take place concomitantly in their electrochemical behavior (57). First, the double layer capacitance is reduced because of their small area relative to that of conventional macro-electrodes. Second, the electrolysis current for the substrate is also smaller, because this parameter is proportional to the electrode dimensions. Third, the effects of ohmic drop are significantly less at nanoelectrodes than at macroelectrodes, since the current generated at nanoelectrodes tends to be small. Consequently, the severe distortion brought by solution resistance to electrochemical data could be greatly reduced.

Hrapovic and Leuong have fabricated a glucose biosensor with a nanoelectrode tip between 10 and 500 nm (59). The biosensor exhibited a picoamperometric current response within 2 s and a detection limit of 20 μM. Single nanoelectrode has also been proven to be able to measure rapid electron transfer kinetics due to a fast response time and a minimum double-layer charging effect (58).

3.4.4. Nanoelectrode ensembles and nanoelectrode arrays

The signal obtained from single nanoelectrode is so small and vulnerable to the interference of the instrument noise. Therefore, a collection of individual electrodes in a NEA operate in parallel to increase the signal intensity. Larger area of NEA will allow more individual electrodes on a single chip to obtain stronger signal. For a low-density NEA with large inter-electrode spacing, the diffusion profiles surrounding individual electrodes are independent of each other. Such a NEA shows a sigmoid-shaped voltammogram, which achieves the maximum current density and highest signal-to-noise ratio (60). For a high-density NEA, the diffusion profiles overlap with each other, leading to a peak-shaped voltammogram. Even in this case, the NEA still shows much higher signal-to-noise ratio than macroelectrodes, because the Faradaic current (I_F), the signal, is dependent on the geometric area (A_{geo}) while the capacitive current (I_c), the background level, is dependent on the total active electrode area (A_{act}) (61). Given an equivalent geometry area for the NEA and the macroelectrode, the signal/background current ratio of a N, $(I_F / I_C)_{NEA}$, is expressed by (61)

$$\left(\frac{I_F}{I_C}\right)_{NEA} = \left(\frac{I_F}{I_C}\right)_{MAC} \bullet \frac{A_{geo}}{A_{act}} \qquad (1)$$

For a NEA composed of the hemisphere electrodes (electrode radius=50 nm, spacing=1 μm), the A_{geo}/A_{act} value is about 3200. Previous experiments have shown that the NEEs with the A_{geo}/A_{act} values between 10^3 and 10^2 have exhibited the detection limit 2~3 orders of magnitude lower than macroelectrode counterparts (62,63).

Martin and co-workers have prepared an ensemble of gold nanodisk electrodes in which the nanodisks have diameters as small as 10 nm (62). Cyclic voltammetric results demonstrated that the detection limits for electroactive species at NEEs containing 10 nm-diameter gold disks could be 3 orders of the magnitude lower than those at the gold macroelectrodes. It was found that if they are of the same geometric area, the net Faradaic current at the NEE is equivalent to that at a macroelectrode, which indicates that the flux at the individual elements of the NEE is many orders of magnitude larger than the flux at the macroelectrode. The higher fluxes at the NEE elements proved that the NEEs were more sensitive to the kinetics of electron transfer than a macroe1ectrode (64,65).

A NEA based on vertically aligned multiwalled carbon nanotubes (MWNTs) embedded in SiO_2 was constructed for ultrasensitive DNA detection (66). Oligonucleotide probes were selectively functionalized to the open ends of carbon nanotubes. By combining such a nanoelectrode platform with Ru $(bpy)_3^{2+}$ mediated guanine oxidation, a detection limit lower than a few attomoles of oligonucleotide targets was achieved. The design of this nanoelectrode array took advantage of the fast electron transfer both at the open end and along the tube axis of a MWNT.

4. SPR BIOSENSORS

SPR arises from the collective oscillation of conduction band electrons in resonance with the incident radiation field (67). The resonance frequency depends on particle size, shape, dielectric constant/refractive index of the surrounding medium, the material composition and *etc*. (67,68). Some noble metals, especially Au and Ag, have SPR band at the visible light region (69). As a result, Au and Ag shows visual color effects from the shift of plasmon band. The model theory is well developed by Mie to understand the physical essence of the plasmon of noble metals (70). SPR biosensors have been designed to detect toxic metal ions, small molecules and biomacromolecules mainly based on the two mechanisms: (i) localized plasmon resonance coupling-induced plasmon band shift due to the aggregation of NPs, and (ii) local dielectric constant/refractive index change-induced plasmon band shift due to addition of analytes (Figure 5). So far, nanoparticles and chips have been extensively investigated as the SPR transducers of sensors.

4.1. Nanoparticle-based SPR biosensors

Here, nanoparticle refers to nanosphere (NS), nanowire (NW) and nanotube (NT). Surface plasmon originates from the large electromagnetic field around NPs, which exponentially decays away from the surface of NPs (71). Plasmon resonance coupling by aggregation of particles results in the peak position shift, visually the colorimetric response. The colorimetric biosensors are

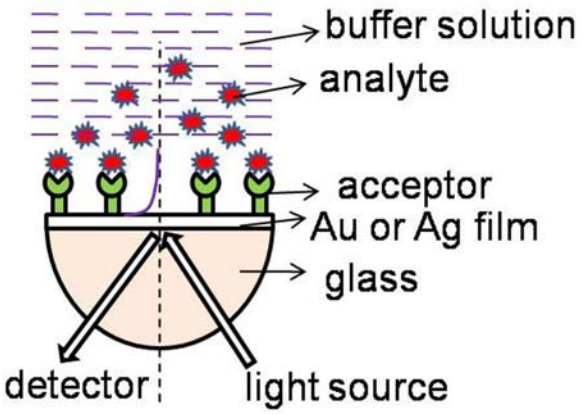

Figure 5. Schematic illustration of surface plasmon resonance biosensor.

extremely attractive because of its simplicity and low cost. It is well-known that the SPR peak position is related to the refractive index of the surrounding medium, since the Mie theory predicts that SPR occurs when Re (ϵ (ω)) = -2ϵ_M where Re (ϵ (ω)) is the real component of the metal dielectric constant and ϵ_M is the medium dielectric constant (72). Therefore, in addition to the colorimetric sensing through the SPR coupling in the aggregated NPs, targets of interest can also be detected through the SPR response from the refractive index change. This sensing approach offers many desirable characteristics including: (i) high refractive index sensitivity, (ii) long-range sensing length scale (200 nm) determined by the exponential decay of the evanescent electromagnetic field, (iii) multiple instrumental modes of detection (angle shift, wavelength shift and image), (iv) real-time detection on the 0.1-0.001 s time scale for measurement of binding kinetics, (v) lateral spatial resolution at the order of 10 μm, enabling multiplexing and miniaturization, and (vi) commercially available instruments (71).

Many groups have developed the colorimetric biosensors using engineered Au NPs or Ag nanoparticles (Ag NPs) (73-76). Mirkin *et al.* have developed DNA/Au NPs probes to detect heavy metal ions including Cu^{2+}, Hg^{2+} and Pb^{2+} (73). These probes exhibited high sensitivity ranging from ppm to ppb level, and high selectivity as well. In these probes, Au NPs were modified by two different single strand DNAs, respectively. Addition of another single strand DNA results in the specific recognition for heavy metal ions.

In general, small molecules are difficult to be detected by the conventional SPR technique because the binding event of small biomolecules only brings in small change of the refractive index, and thereby the low sensitivity. However, Zhou *et al.* have reported an aptamer/Au NPs assembly system for sensitive detection of adenosine (77). In their system, the aptamer firstly immobilized onto the Au film could hybridize with its complementary single strand DNA attached onto Au NPs. Addition of adenosine caused change of the aptamer structure, and thereby it could not hybridize with DNA attached onto Au NPs. The change of aptamer structure significantly affects the refractive index at the interface between Au NPs and media, which resulted in a large change in the SPR signal. The change in the SPR signal proportionally decreased with an increase in the concentration of small molecules. Recently, graphene was used as the support of Au NPs to enhance the sensitivity (78). The improved performance of graphene-Au system originated from the unique structural and optical natures including: (i) strong adsorption affinity for biomolecules due to the carbon-based ring structure of graphene and (ii) enhanced SPR sensitivity due to change of the refractive index.

Both theory and experiments suggest that anisotropic shapes, especially nanorods of Au NPs and Ag NPs, show higher SPR sensitivity in comparison with the symmetric NSs (67,69,79). Au or Ag nanorods exhibit two SPR bands, which are the transverse mode along the width of the rod and the longitudinal mode along the length of the rod, respectively. Both bands are tunable with the aspect ratio (the length to the width). In addition, the longitudinal SPR band has been observed in the range from 500 nm to 1600 nm, and is more sensitive to the refractive index in comparison with the transverse one. Au and Ag nanorods have distinct advantages over the NSs in the biosensing, including (i) tunable surface plasmon resonance band by the aspect ratio of nanorods, (ii) the near infrared plasmon band applicable for the biological sensing with non-damage penetration into tissue, (iii) high longitudinal SPR band sensitivity to the surrounding environment, and (iv) the distinct chemical reactivity between the end and the middle of nanorods (67).

Yu and Irudayaraj have reported the multiplexed biosensor using Au nanorods (79). Au nanorods with various aspect ratios (2.1, 4.5 and 6.5) exhibit significantly distinct sensitivity of longitudinal peaks to the refractive index change in their vicinity. Three different recognition agents (monoclonal human IgG1 Fab, monoclonal mouse IgG1 Fab and monoclonal sheep IgG (H+L)) were attached onto the Au nanorods with the aspect ratios of 2.1, 3.5 and 6.5, respectively, producing Probe 1, Probe 2 and Probe 3. And then monoclonal goat anti-human IgG Fab, monoclonal rabbit anti-mouse IgG Fab and monoclonal rabbit anti-sheep IgG (H+L) were immobilized onto three probes, respectively. The significant distinct red-shift of longitudinal plasmon peaks in three probes was observed, which enabled the detection of three targets simultaneously. It is worth noting that red-shift of the longitudinal SPR band was not ascribed to the aggregation of NPs but the change in the refractive index resulting from the target binding event.

It has been found that noble metals with various shapes such as nanoflowers, nanodendrites and nanotriangles show strong SPR absorption, which results from the concentrated electromagnetic fields in the sharp tip and the rough surface structure (80-82). Nevertheless, these structures were seldom used for SPR biosensing, since the complicated structure renders difficulty for analysis of the system.

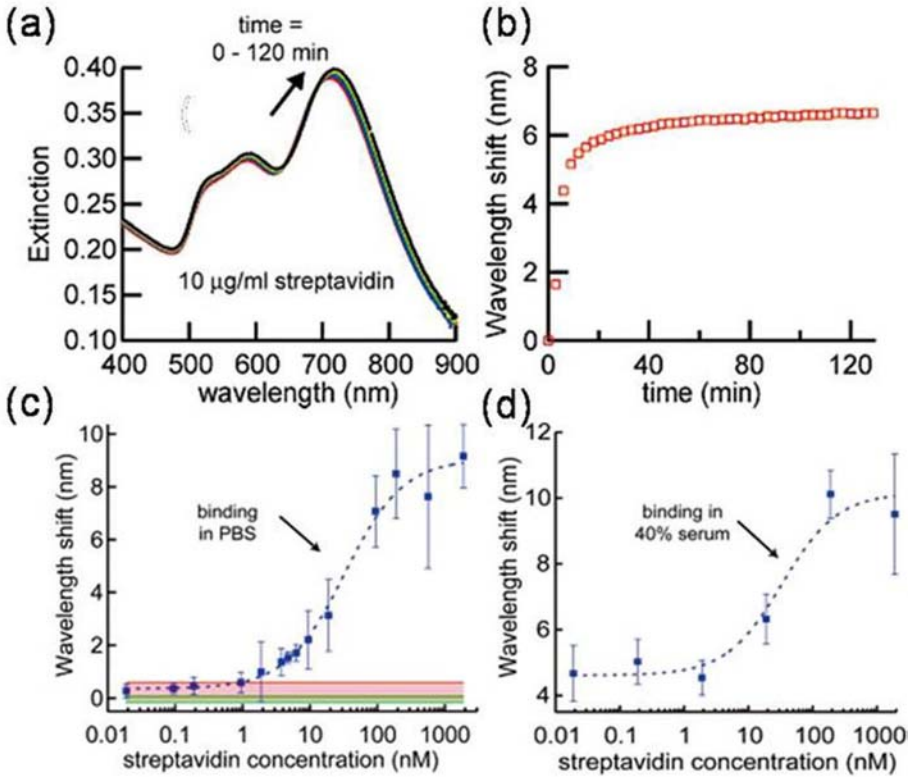

Figure 6. (a) Observation of streptavidin binding to biotin at the surface of the gold nanorods using UV-vis spectroscopy, (b) wavelength shift vs streptavidin incubation time, (c) Dose-response curve for biotin-streptavidin binding at the nanorod surface in PBS. The error bars represent the 95% confidence interval associated with each concentration. The green bar represents $\pm 3\sigma$ instrument noise. The red bar represents the average shift ± the standard deviation of the sensor response to 10 μg/mL BSA and 10 μg/mL biotin-saturated streptavidin. (b) Dose response curve for biotin-streptavidin binding in 40% serum. The error bars represent the standard deviation calculated from at leastthree independent measurements. Reproduced with permission from (84).

4.2. Chip-based SPR biosensors

The setup for chip-based biosensing is typically constructed with the Kretschmann configuration (Figure 5), which measures the reflectivity of the noble metal film at various angles (68). The surface modification provides the specific chemistry to bind targets of interest. The binding of targets on the substrate induces a small and measurable change in the frequency of SPR resonance band, depending on the substrate composition and morphology, the surrounding medium, target and its surface coverage. So far, efforts have been focused on making highly sensitive SPR substrates. It has been noticed that smooth noble metal films do not show strong surface plasmon absorption. However, when Au or Ag was deposited over monodisperse polystyrene or SiO_2 nanospheres to form a film over the nanospheres (FON) surface, the FON substrate shows strong SPR absorption (83). The thickness and the interlayer spacing affect the position of the SPR band. The thicker metal film and the wider spacing result in red-shift of the SPR band (69).

Various shapes such as NS, nanorod and nanocube have been extensively used to make SPR films. As shown previously, the anisotropic structure is a better alternative for biosensing based on SPR (79). It is reasonably expected that nanorod chips have a lower limit of detection in comparison with NS chips. Chilkoti *et al.* have compared the nanorod chip-SPR biosensor with the NS chip-SPR biosensor (Figure 6) (84). Au nanorods and Au NSs were chemisorbed onto a mercaptosilane-modified glass substrate, respectively, followed by conjugation of biotin. Addition of streptavidin caused a red-shift of SPR band or an extinction increase due to the biotin-streptavidin binding interaction. The limit of detection of the Au nanorod chip was 94 pM in PBS and 19 nM in serum, which was better than that obtained by Au NS in PBS (0.83 nM).

In addition to the nanorod structure, the anisotropic substrate patterned with nanotriangle, nanodot, nanocube and nanohole arrays are also robust plasmonic materials (68,85,86). These structures can be prepared by the well-established nanosphere lithography. The SPR position can be tuned by changing the size, shape or spacing of the nanoarray. Moreover, these patterns with different shapes exhibit distinct sensitivity for SPR biosensing. El-Sayed *et al.* have investigated the localized SPR of Au nanodisc pairs, and found that the fractional plasmon wavelength shift polarization along the interparticle axis decays nearly exponentially with the

interparticle gap, and the decay length is roughly 0.2 in units of the particle size (85). The plasmon shift can be derived from the empirical equation (called plasmon ruler equation): $\Delta\lambda/\lambda \approx 0.18 \exp(-(s/D)/0.23)$, where $\Delta\lambda/\lambda$ is the fractional plasmon shift, s is the interparticle edge-to-edge separation, and D is the particle diameter. Masson *et al.* have prepared a series of triangle arrays and microhole arrays using modified nanosphere lithography (68). Such nanohole array-based sensors exhibited a low detection limit of 10 nM for IgG. It was found that the nanohole array possessed excellent refractive index resolution (10^{-6} RIU), high sensitivity to refractive index variation (>3000 nm/RIU) and monolayer formation (2-fold improvement compared to thin films).

5. SERS BIOSENSORS

Raman spectroscopy is a versatile technique for molecule identification by providing the fingerprint information of chemical and biological species. However, Raman signal is very weak due to the low inelastic light scattering event and cannot be used as an efficient biosensing technique until Fleischmann and his colleagues discovered the enhanced Raman scattering in 1974 when pyridine was adsorbed onto a roughened silver electrode (87). Although the enhancement mechanism still is in debate, it is accepted that the electromagnetic (EM) and the chemical (CM) enhancement mechanisms contribute to SERS (88-90). Both mechanisms coexist in most of SERS systems but the contribution of CM mechanism is significantly lower than that of EM. The CM enhancement results from the charge transfer between substrate and chemisorbed molecules. As for the EM mechanism, the interactions between the metallic nanostructures and the incident electromagnetic field can lead to significant SPR bands in the local electric field at the surfaces of the nanostructures. These SPR bands significantly amplify SERS signal. The SERS can be enhanced by a factor proportional to the fourth power of the enhancement of the local incident near-field. Generally, metals with high optical reflectivity such as silver, gold and copper, which exhibit negative values of the real part and small values of the imaginary part of the dielectric constant, are ideal SERS materials. Transition metals such as Fe, Ni, Pd and Pt that have low optical reflectivity do not satisfy the requirement for efficient SERS effect. Based on the EM theory, the size of the metal particles is required to be much smaller than the wavelength of the exciting radiation (Rayleigh approximation).

Figure 7 gives a good example to demonstrate the sensing principle of SERS biosensors (95). When the analyte target is capture by the molecular probes that are linked to the Ag nanoparticles and the Ag film, a SERS-active nanostructure is created, generating the SERS signal of the surface-bounded Raman label. SERS has been used for detection of chemical and biological species at the single molecule level (91-95). The material composition, size, shape and surface roughness impose great effects on the surface plasmon peak position, intensity and distribution, and thus affect the SERS signal (96). In general, stronger electromagnetic field and the resulting higher SERS appears on the location close to the sharper and rougher surface. These structures with such SERS features are extremely desired.

SERS-based biosensors have some advantages over fluorescent, SPR, and electrochemical biosensors (97) including (i) label-free detection, (ii) excellent reproducibility, (iii) more reliable multiplexing capability because of finger-printing Raman spectra, (iv) much higher sensitivity, and (v) potentially greater flexibility due to larger pools of available and non-overlapping Raman reporters.

5.1. Nanoparticle-based SERS biosensors

Local electromagnetic field is significantly enhanced at the gap between two particles, the so-called "hot spot", which allows SERS enhancement factor to increase up to 10^{12}-10^{15} (98). Therefore, the nanostructures with sharp or rough junctions are preferable for SERS-based biosensors. At present, the conventional approach is to obtain the condition-controllable aggregation of Au NPs or Ag NPs. The Raman reporter tags positioned at the "hot spot" can respond to the enhanced electromagnetic field, and thereby result in the SERS activity.

Highly active SERS nanostructures, including engineered dimers and trimers, can be obtained by the advanced synthetic chemistry and nanofabrication techniques (99,100). These homogeneous and reproducible structures further allow making high quality biosensors with expected detection limit. Bell and Sirimuthu have used citrate-coated Ag NPs as the SERS substrate to determine the sequence of the DNA/RNA mononucleotides in the presence of $MgSO_4$ (101). The Ag NPs without any modification were just directly added to the solution containing mononucleotides. The cation Mg^{2+} induced the aggregation of the Ag NPs, and mononucleotides existing at the gap between the Ag NPs exhibited the enhanced Raman signal, leading to a detection limit at ppm level. Therefore, the direct injection of Au NPs or Ag NPs into the biological cell resulted in the *in-situ* detection of biomacromolecules. Lee *et al.* have developed a SERS-active platform through self-assembly of DNA-functionalized Au NPs and Au NWs (102). Au NPs were functionalized by Raman reporter-labeled single strand DNA while Au NWs were functionalized by another DNA. After adding the complementary DNA, one end of the target DNA bound to DNA adsorbed on the Au NPs while the other end of target DNA bound to DNA on the Au NWs. Thus, the Au NP-DNA-Au NW sandwich architecture was formed to create the "hot spot". Raman signal from Raman reporter existing in the "hot spot" was significantly enhanced. This system was demonstrated to be sensitive and specific for pathogen DNA targets with the detection limit at the pM level. It has a potential for diagnostics of infection diseases.

Nanostructures with high roughness, like nanostars, nanoflowers and nanotriangles, have also been used as SERS platforms, which bring high enhancement factors (103-105). In addition, the composite materials with core/shell structures are able to amplify the local

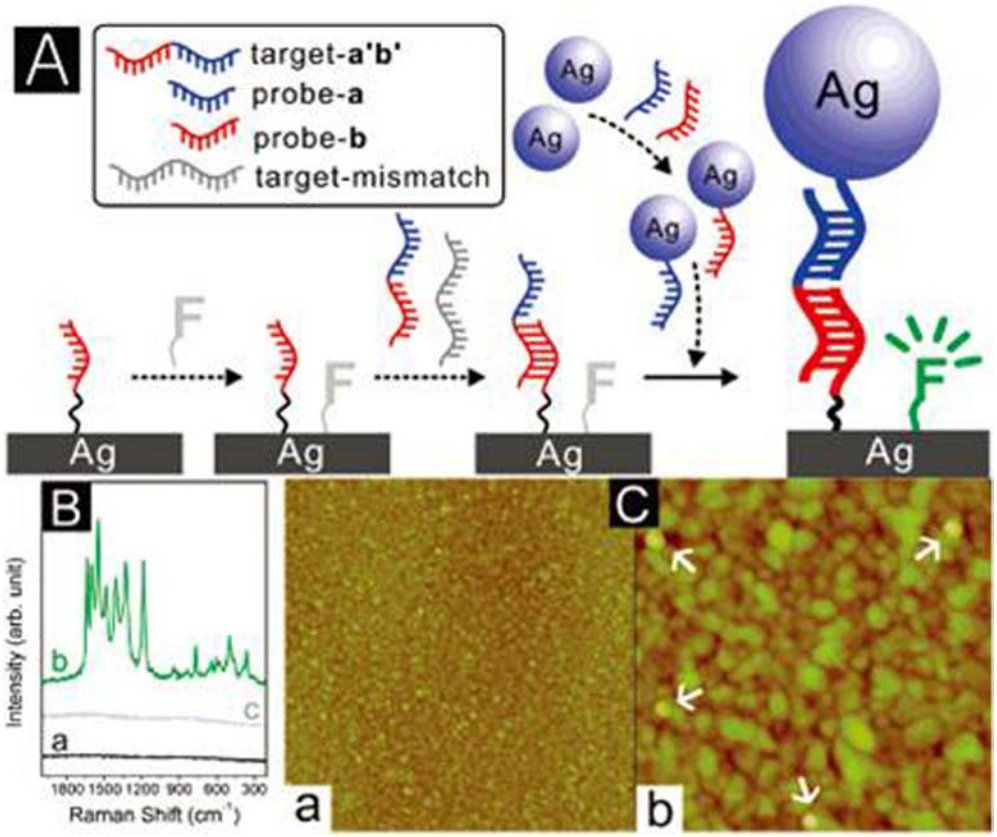

Figure 7. (A) Schematic illustration for the detection of single-stranded DNA by SERS. A target strand (a'b') is captured by probes on AgNP and AgFilm-F, resulting in the creation of the SERS-active structure in the form of a-AgNP/a'b'/b-AgFilm-F. Target DNA detection is confirmed by collecting the SERS signal of surface-bound Raman label, F. (B) SERS spectra (vertically offset for clarity) obtained from (a) of a'b'-anchored b-AgFilm-F, (b) a-AgNP/a'b'/b-AgFilm-F, and (c) prepared similar to b except for a noncomplementary target sequence in place of a'b'. (C) Representative AFM images of a-AgNP/a'b'/b-AgFilm-F: (a) 5 μm 5 μm and (b) 1 μm×1 μm. Arrows point to AgNPs on the surface. Reproduced with permission from (95).

electromagnetic field, and even induce the fast, efficient electron transfer for the chemical enhancement of Raman signal (106). However, the stability and the homogeneity of nanomaterials still remains a challenge, which may influence the reproducibility of Raman signals.

5.2 Bead-based SERS biosensors

Besides Raman reporters were directly adsorbed onto the surfaces of NSs, NWs and NTs, they are also embedded into beads for multiplexed bioassay (97,107-109). This brings in: (i) long-term stability and reproducibility, (ii) less side reaction, (iii) great enhancement in signal of given analytes, (iv) facile surface functionalization for immobilization of biomolecules, and (v) no leakage of Raman reporters (97,109).

Several approaches were used to obtain the beads that are encoded by multiple Raman reporters for signal amplification. Raman reporters were either encapsulated into the core or the shell layer. In Nie group's work, Raman reporters (organic dyes) were incorporated into the SiO_2 shell layer with a Au NP as the core (107). The organic dyes containing the isothiocyanate group can be homogeneously dispersed into the SiO_2 shell. The organic dye-engineered Au/SiO_2 core-shell nanomaterials could avoid the problems including surface adsorption, substrate variations and poor reproducibility, and paved a novel way for multiplexed detection of biomarkers. The Raman reporter-embedded SiO_2 layer functionalized with carboxyl or amino groups can easily bind to biomolecules, and thereby are applied to the SERS-based biological imaging. Wang *et al.* have investigated the Au/SiO_2 beads for detection of pesticide residues on fruits, yeast cells and other small molecules (108). In addition, Zhang *et al.* found that the Raman reporter-embedded SiO_2 core-Au shell beads exhibited giant enhancement of SERS, which is probably ascribed to the fact that the nanoshell acts as a cavity to concentrate the electromagnetic field (110).

SERS-encoded hollow particles, which typically exhibit enhanced SERS, are another kind of efficient structure for biological assays. Alvarez-Puebla *et al.* have prepared Au NP-encapsulated SiO_2 hollow particles, which were encoded by benzenethiol, 4-nitrobenzenethiol or 4-hydroxybenzenethiol (Figure 8) (97). After adding the antibody-modified Ag NPs, the antibody-capsule conjugates were specifically bound to the antibody-Ag conjugates. Thereby the SERS signal from encoding

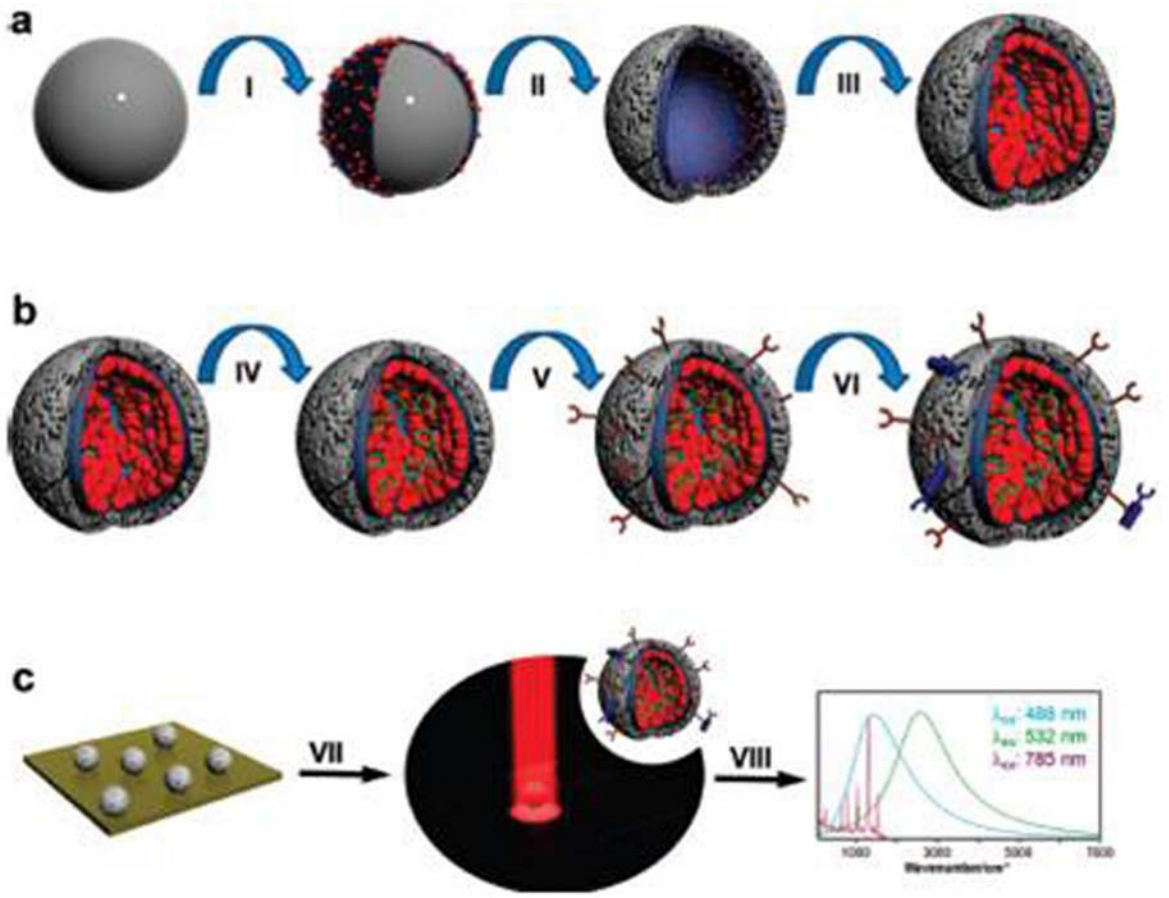

Figure 8. Schematic illustrations of the Multistep (a) Fabrication and (b) Codification, Biofunctionalization, and Biosensing Procedures[a] and of (c) the Biosensing Assay[b] . [a] (I) Polyelectrolyte coating of PS beads and Au seed deposition; (II) PVP wrapping, silica coating, and PS dissolution; (III) seeded Au NP growth; (IV) SERS probe diffusion; (V) antibody attachment; (VI) antigen biorecognition. [b](VII) Illumination of the capsule mixture with different laser lines; (VIII) spectral deconvolution. Reproduced with permission from (97).

species was obtained. Multiplexed detection of biotargets can be realized with the mixed Raman reporters. Six dissimilar DNA targets were simultaneously detected by the use of six Raman-labeled Au NP probes. The resulting SERS probes exhibited a detection limit of 20 fM (109).

5.3 Chip-based SERS biosensors

A small area of chip can provide a SERS biosensing platform with multiplexed detection capability and improved flexibility. Reich *et al.* have reported a biosensing strategy based on SERS in order to detect the DNA sequence (111). They added the DNA/Ag NP conjugates to the DNA-functionalized Ag film modified by Raman dyes. The smooth Ag film produced only low SERS enhancement. After the DNA-modified Ag NPs were added, the single strand DNA complementarily bound to the DNA strand adsorbed on the Ag film. As a result, the hot spots were created, leading to enhancement of the Raman signal.

It is well known that rough surface structure concentrates the electromagnetic field, and thereby benefits to SERS. Van Duyne group have investigated SERS biosensing for biowarefare agent using Ag FONs for the first time (Figures 9 and 10) (83, 111). The characteristic down-concave structure among those spheres provides the strong electromagnetic field for SERS. The detection of *Bacillus subtilis* spores was conducted through the extraction of calcium dipicolinate, a biomarker for *bacillus* spores. It was found that the limit of detection reached 2.1×10^{-14} M, which was below the anthrax infectious dose of 10^4 pores.

Arrays of various nanopatterns have been used for SERS detection. These nanopatterns include nanoflowers, nanoholes, nanodots and nanotriangles of Ag or Au on silicon or glass substrates, and are extremely stable (112,113). Typically, the surface plasmon resonance absorption bands red-shift in order of sphere < cylinder < cube < prism < pyramid. The surface plasmon distribution surrounding the patterns varies as a function of its geometry. The strongest electromagnetic field appears near the sharp tip. Crozier and co-workers reported a double-resonance SERS substrate, showing advantages over conventional single-resonance structures (114-116). The double-resonance substrate consisted of a Au or Ag disk

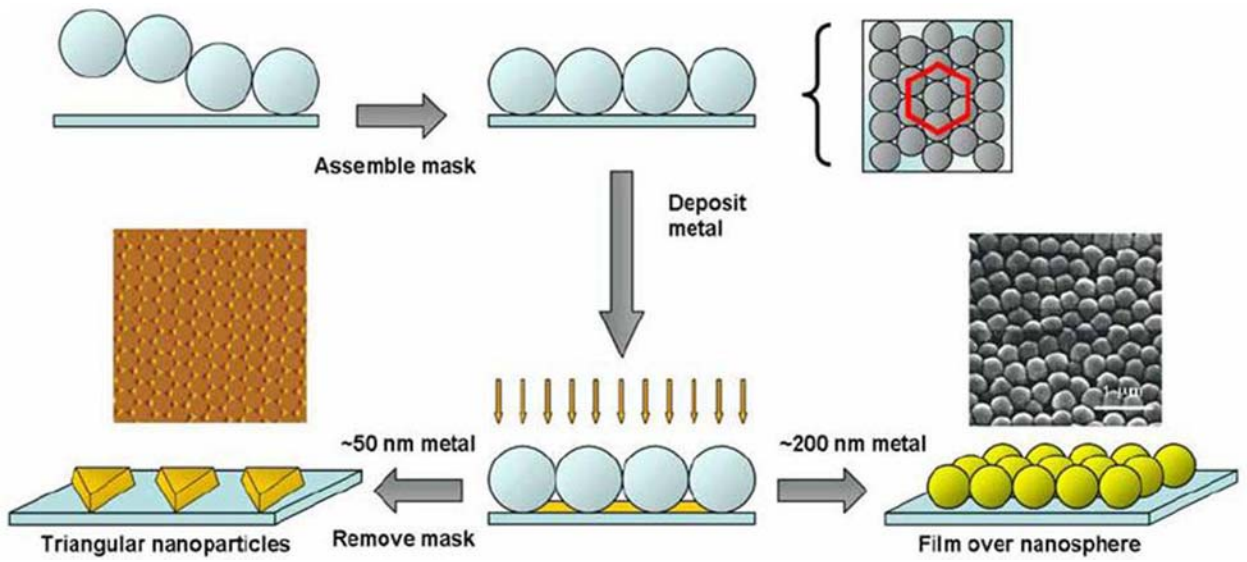

Figure 9. Nanosphere lithographic fabrication of nanoparticle arrays and film over nanosphere surfaces (FON). Reproduced with permission from (83).

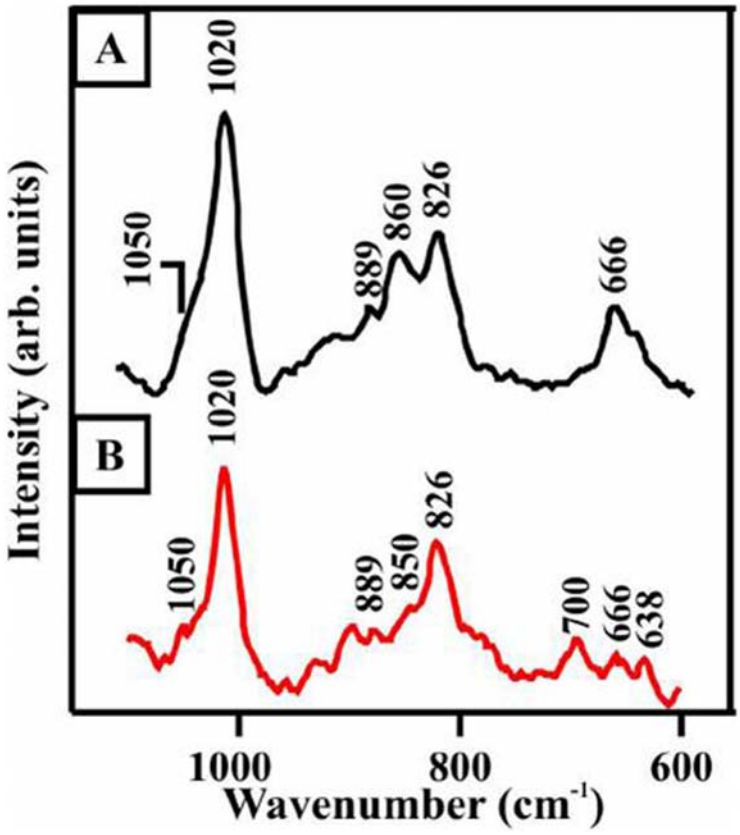

Figure 10. SERS spectra obtained by portable Raman spectrometer. (A) SERS spectrum of 8.3×10^{-14} M spore suspension (1.0×10^4 spores in 0.2 µL, 0.02 M HNO_3) on 30-day old AgFON. (B) SERS spectrum of 10^{-4} M CaDPA in 0.2 µL 0.02 M HNO_3 on 30-day old AgFON substrate. λ_{ex} = 785 nm, P_{ex} = 35 mW, acquisition time = 5 sec, resolution = 15 cm-1, D = 600 nm, and dm = 200 nm. Reproduced with permission from (83).

array, a SiO_2 spacer and a continuous Au film. The strong coupling interaction between localized surface plasmon and propagating surface plasmon contributed to the enhancement of the local field and the double-resonance feature in extinction spectra. The SERS enhancement factor of double-resonance structure was more than two orders of magnitude higher than that of a Au disk array on the glass substrate. The largest SERS enhancement factors for the Au device and the Ag device were 7.2×10^7 and 8.4×10^8, respectively. In addition, Bazan *et al.* have developed a SERS-active platform to detect multi-analytes simultaneously in a single bioassay (117). The Ag micropad was prepared on the silicon surface, and then functionalized with a mixture of three different aptamers. The three aptamers can specifically bind to three proteins, that is, human α-thrombin, platetlet-derived growth factor-BB and immumoglobutin E, respectively. Three different Raman reporters were chemically adsorbed onto the Ag NP surface. After each protein was specifically bound onto the corresponding aptamer, three different Raman reporters labeled Ag NPs were incubated in the aptamer-modified Ag mircopad, and recognized by aptamers. Thus, the aptamer-Ag mircopad/protein/Raman reporter-Ag NP sandwich architecture was formed, leading to the SERS signal. This sensor yielded a limit of detection of 100 pM.

6. FLUORESCENT BIOSENSORS

Organic fluorophore-based biosensors have been extensively studied in the past forty years, and are currently the most popular technique for the clinical diagnostics and detection of various targets (118, 119). However, most of organic fluorophores have shortcomings such as narrow excitation profile, nonsymmetrical emission spectra and photobleaching (120,121). Since 1990s, inorganic semiconductor nanocrystals (quantum dots, QDs), metallic cluster fluorophores and organic-inorganic composites have emerged as novel fluorescent labels in biosensing and imaging, and are substituting the conventional organic fluorophores. This is ascribed to great advantages of inorganic nanocrystals over the conventional organic dyes. Semiconducting QDs exhibit broad excitation profiles, narrow and symmetric emission spectra, high photostability and high quantum efficiency and excellent multiplexed detection capability (120,121). For example, QDs with different emission wavelengths can be excited by single excitation source while organic dyes with different emission wavelengths must be excited by multiple excitation sources. Demand of simultaneous detection of more targets in single assay drives the development of inorganic nanocrystal-based fluorescent probes to replace organic fluorophores (18,120,122-126). This section will deal with these novel fluorophores including QDs and metallic clusters for biosensing applications.

6.1. Nanoparticle-based fluorescent biosensors

Chalcogenide QDs are enxtensively used in fluorescent biosensors. However, they are toxic and hydrophobic. Recent development of synthetic chemistry has allowed preparing water-soluble QDs with mitigated toxicity (127-129). The strategy developed for enabling biocompatibility is to modify the surface of QDs with more biologically friendly coatings such as 3-mercaptobenzoic acid (MPA), dihydrolipoic acid (DHLA), HS-poly (ethylene glycol)-carboxyl acid (HS-PEG-COOH), or other hydrophilic and bifunctional ligands.

The size-tunable optical properties allow QDs to act as optical acceptors as well as donors for biosensing based on Förster resonance energy transfer (FRET) (130, 131). FRET is a process that involves nonradiative energy transfer from a donor in its electronic excited state to an acceptor through dipole-dipole interactions. The acceptor will be relaxed to its ground state through emitting photons or releasing heat energy. The FRET efficiency strongly depends on the separation distance between donors and acceptors. In general, FRET sensors require the separation of absorption profile of acceptors from the emission of donors to avoid the direct excitation (121, 132).

Mattoussi group and Willner group have pioneered this area for detection of biomacromolecules, toxic metal ions and hazardous explosives, etc. Mattoussi and co-workers have linked single-chain antibody fragments to the surface of DHLA-modified QDs (CdSe/ZnS core/shell) (Figure 11) (133). This antibody was pre-bound by a dye-labeled 2,4,6-trinitrotoluene (TNT) analogue. Exposure to the solution containing TNT resulted in displacement of TNT analogue pre-bound in the antibody binding site away from QDs, thereby the recovery of fluorescence emission of QDs. This system exhibited a limit of detection of 20 ng/mL for TNT. The excellent specificity of this assembly for TNT was demonstrated by examining three other analogues (Tetryl-DNT, 2,-A, 4,6-DNT and 2,6-DNT). It was reasonably expected that this system had the potential for multiplexing detection of targets through the use of QDs with different emission wavelengths. Willner and co-workers adopted the similar structured assembly to investigate hybridization and cleavage of DNA (134). DNA/QDs conjugates were initially hybridized with the complementary Texas Red-labeled DNA. Addition of DNase I resulted in the cleavage of DNA, and successively the partial recovery of fluorescence emission of QDs. The previous studies used organic dyes as quenchers, which have promoted the development of biosensing. It is well known that toxicity and photo-degradation of dyes cause the environmental risk and low reproducibility issue. Fortunately, Au NPs have been demonstrated to be more efficient quenchers than those conventional organic dyes (135-137). The nonradiative quenching of QDs emission by Au NPs is due to long distance dipole-metal interactions that extend significantly beyond the classical Förster distance (~6 nm). The quenching efficiency strongly depends on the particle size (138). The quenching constant increases with increase in the Au NP size, because the absorption cross-section of Au NPs is the main parameter affecting the energy transfer efficiency. The assembly with QDs as the donor and the Au NP as acceptor is extremely attractive for bioassays. Grant and co-workers have assembled the biosensor with fluorophores as the energy donor and Au NPs as the energy acceptor, modified by specific capture antibody (139). This

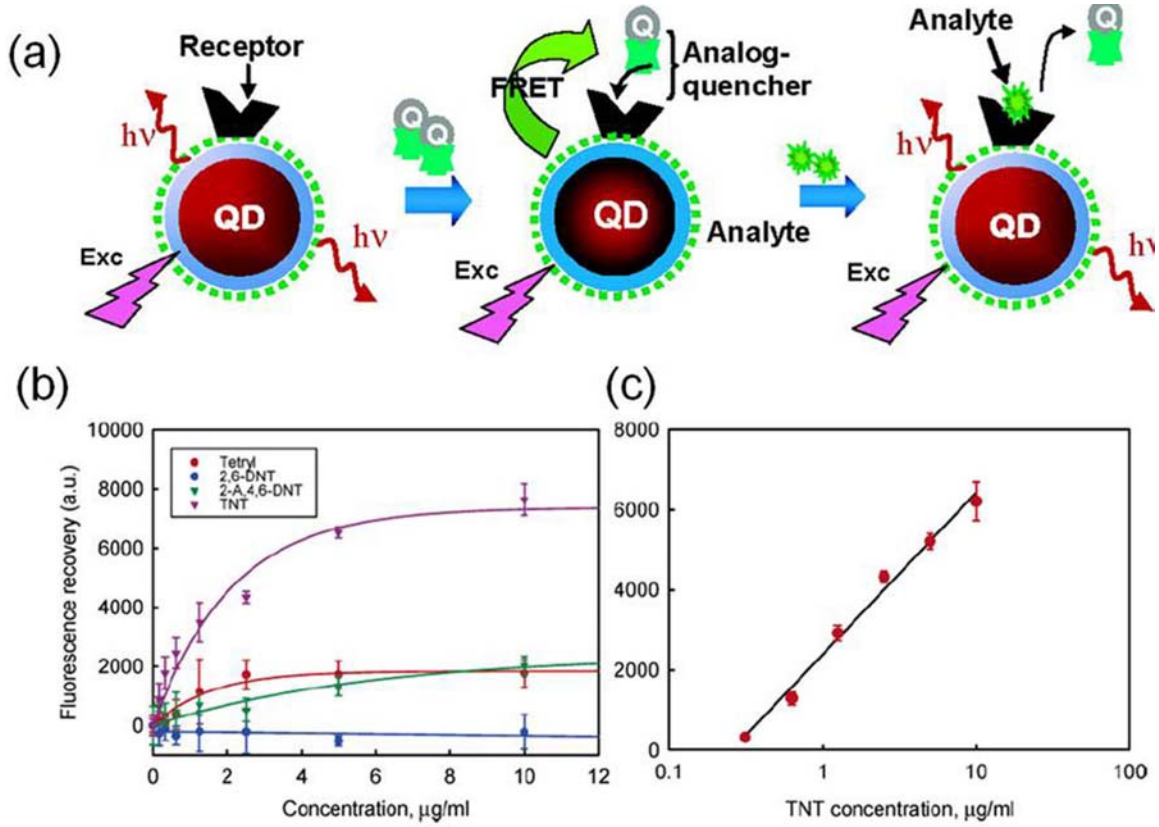

Figure 11. TNT titration of QDs-TNB2-45 nanosensor assembly. (a) Schematic of assay. When TNB-BHQ-10 is bound to the QD-TNB2-45 conjugate, QD fluorescence is quenched. As TNT is added to the assay, it completes for binding to the antibody fragment and the QD fluorescence increases following TNB-BHQ-10 release from the conjugate. (b) Results from titration of the QD-TNB2-45-TNB-BHQ-10 assembly with TNT and the indicated TNT analogues. (c) Curve constructed from titration of QD-TNB2-45-TNB-BHQ-10 nanosensor assembly with a TNT standard. These assemblies were constructed using 530 nm emitting QDs. Each data point is an average of three measurements, and error bars represent the standard deviation. Solid lines are guides to the eye drawn through the experimental points. Reproduced with permission from (133).

assembling was found to be a feasible method for Porcine Reproductive and Respiratory Syndrome Virus (PRRSV) detection with the detection limit of 3 particles/µL.

In addition to the semiconductor nanocrystal QDs, Au NPs and Ag NPs with the size down to several atoms to 1-2 nm exhibited high photoluminescence quantum yields with respect to large particles and bulk materials (140,141). Their fluorescence emission wavelength varies from blue to near-IR region. The emission wavelength undergoes a blue shift as the size of NPs decreases. These fluorescent NPs have been employed for detection of heavy metallic ions (140) and small molecules (141), showing the excellent selectivity for Hg^{2+} and a detection limit of 5.0 nM in the presence of 2,6-pyridinedicarboxylic acid (PDCA). But less investigation was conducted to detect biomacromolecules both *in vivo* and *in vitro*, probably due to their unstable structure and difficult modification.

Nanowire- and nanotube-based fluorescent biosensors are attractive for the optical bioassays because of their confined electron transportation along the one-dimension direction. Chen *et al.* have assembled a DNA aptamer probe through attaching thiolated thrombin binding aptamer on Au NWs (142). Exposure of these probes to the biotinylated thrombin led to the specific recognition of targets labeled by fluorescent reporter. The fluorescence intensity from the probe-target-reporter assembly varied as a function of the distance between the fluorophore and the Au NW due to the surface energy transfer. When the positive potential was applied to the Au NW, the fluorophore was attracted toward the NW, leading to the decrease of the fluorescence intensity. When the negative potential was applied to the NW, the fluorophore was repelled away from the surface, which resulted in the recovery of the fluorescence intensity from the fluorophore. This biosensor can detect thrombin at a single molecule level with a limit of detection of 100 fM. It was believed that the electrically modulated fluorescence method can be extended to detection of other targets.

Novel composite nanomaterials, such as QD-carbon nanotubes and QD-graphene oxides, are really

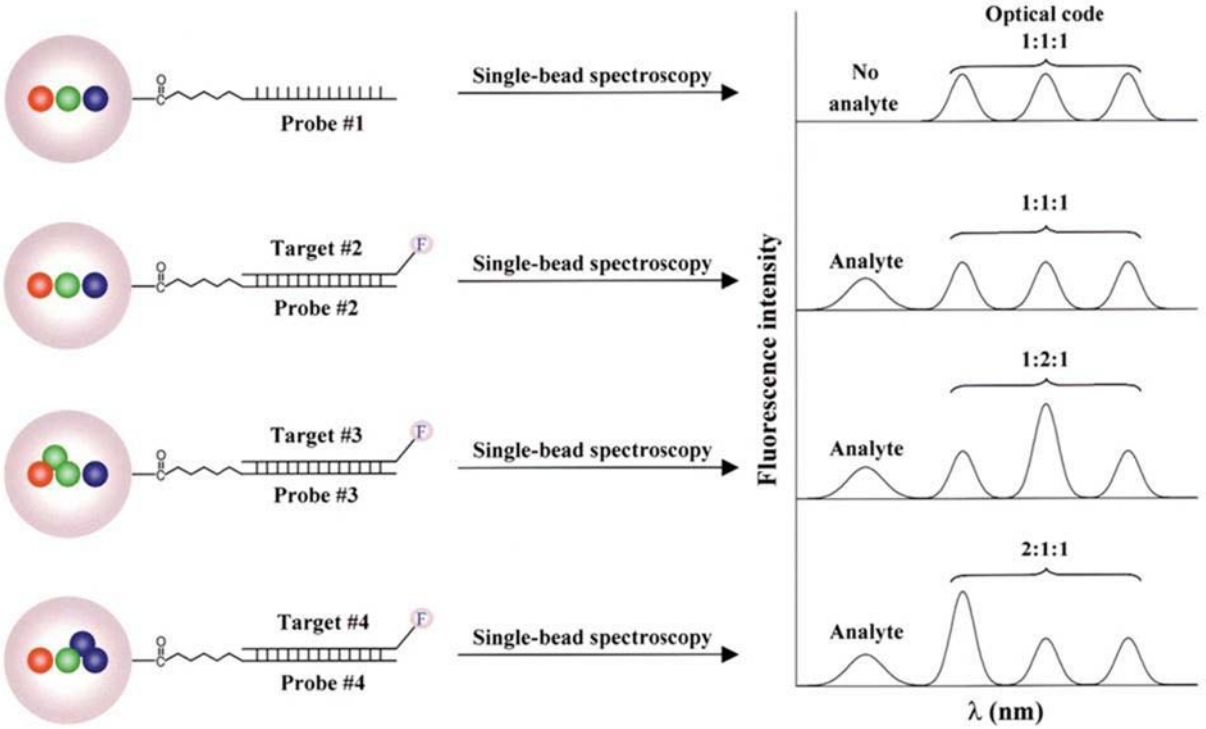

Figure 12. Schematic illustration of DNA hybridization assays using QD-tagged beads. Probe oligos (No. 1–4) were conjugated to the beads by crosslinking, and target oligos (No. 1–4) were detected with a blue fluorescent dye such as Cascade Blue. After hybridization, nonspecific molecules and excess reagents were removed by washing. For multiplexed assays, the oligo lengths and sequences were optimized so that all probes had similar melting temperatures (T_m = 66–99 ^oC) and hybridization kinetics (30 min). Reproduced with permission from (148).

efficient candidates for fluorescent biosensors. Graphene oxide has been extensively studied for biosensors because of its unique characteristics such as facile surface modification, high mechanical strength, good water dispersibility, and photoluminescence (143). The planar structure facilitates the electron and energy transportation in particular. In addition, graphene oxide is also a kind of ideal support for NP loading. Seo and co-workers have reported a graphene oxide-based immuno-biosensor for pathogen detection with high sensitivity and selectivity (143). This sensor was based on the photoluminescence quenching of graphene oxides through the FRET process induced by the Au NPs. The antibody-modified graphene oxides could recognize the pathogen due to the specific antigen-antibody interaction. This system showed a detection limit of 10^5 pfu/mL, which was comparable with that of the conventional ELISA technique. Similarly, carbon nanotubes were demonstrated to be an efficient fluorescence quencher in biosensors (144). The high stability and mechanical strength make carbon nanotubes feasible to be used in the stringent detection environment. Tan *et al.* have reported a hairpin-structured assembly, which consists of oligonucleotide-modified SWNTs and dyes-labeled complementary oligonucleotides (144). Upon the complementary recognition of oligonuleotides, carbon nanotubes quenched the fluorescence emission from the dye tags.

6.2. Bead-based fluorescent biosensors

Fluorophore-embedded beads can contain multiple fluorescent molecules in single entity to achieve high sensitive and high throughput analysis of targets. This strategy exhibits superior characteristics for bioassays (145-147), including: (i) avoiding the leakage of the fluorescent label and resulting long-term stability, (ii) enhancement of the fluorescence intensity and consequently the improved sensitivity, (iii) facile surface functionalization for immobilization of biomolecules. Multiplexed detection can be realized through trapping the fluorophores with different emission spectra into single bead. The multiplexed detection capacity depends on the spectral coding in the bead, which is determined by the intensity level and the color (emission wavelength) number. Theoretically, n intensity levels with m colors generate distinct (n^m-1) codes (148).

Nie and co-workers have used this approach to demonstrate the potential of the QD-embedded beads for multiple spectral coding (Figure 12) (148). Different-sized QDs with different fluorescent emission wavelengths were incorporated into the polymeric microbeads at the precisely controlled ratios. The dye-labeled DNA target was combined with the DNA-functionalized microbeads that contained the QDs at different concentration ratio. Thus the sensing signals for multiple targets can be acquired

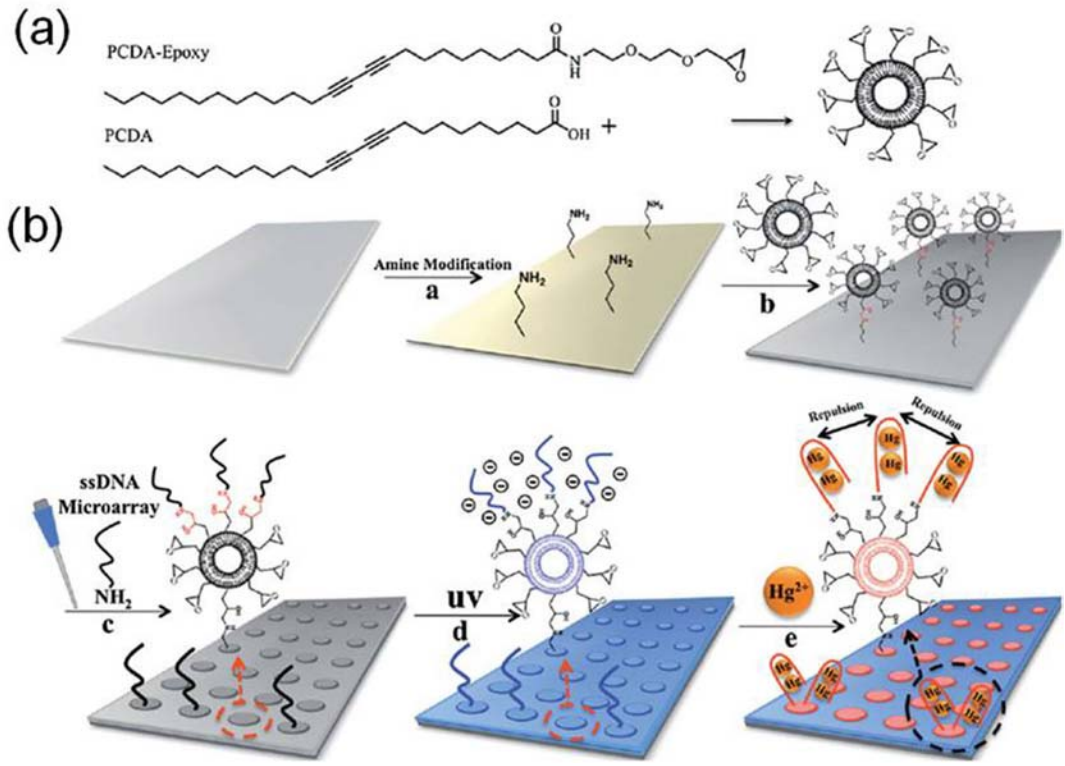

Figure 13. (a) Chemical structure of the diacetylene monomers, PCDA and PCDA-Epoxy. (b) Schematic illustration of the PDA liposome-based microarray for mercury detection. a) Surface modification of the glass substrate with amine functionality. b) Immobilization of the Epoxy liposomes onto the amine glass slide through epoxy-amine coupling. c) Post-tethering of the ssDNA aptamer by means of a microarrayer. d) Photopolymerization of the PDA liposomes using a 254nm UV lamp. e) Recognition of the target mercury ions results in red fluorescent emission. Reproduced with permission from (151).

simultaneously at the single-bead level. This fluorescent platform can be used for high throughput detection of various targets such as DNA, cancer biomarkers and heavy metals.

Nabiev *et al.* have explored the multiplexed detection of circulating autoantibodies, the markers of systemic sclerosis (149). The microbeads coded by three QDs with green, orange and red emissions were functionalized by the antigens, followed by coating of the bovine serum albumin protein. The specific interaction between the microbead and the antibody turned the fluorescence signal from the dye label "off" and "on" through the FRET mechanism. The results demonstrated the promising application of QD-encoded microbeads for multiplexed antibody profiling, clinical diagnostics of autoimmune diseases.

6.3. Chip-based fluorescent biosensors

In two-dimensional bioassays, chips are usually patterned with various nano-scale or micro-scale structures. Chip-based fluorescent assays allow massive detection and screening of targets in a small area and can be integrated with microfuidics to build lab-on-chip systems. Alivisatos and co-workers have successfully deposited the QDs with specific fluorescence emission wavelength on the defined micrometer-sized surface to form the micropattern-containing QDs (150). In this case, the micrometer-size Au pattern was grown on a silicon wafer using the standard lithography technique. The Au pattern provided easy surface chemistry for DNA immobilization. Following this, the QDs of different emission wavelengths were functionalized by the corresponding complementary single strand DNA, respectively. Immersion of the Au pattern chip into the mixed DNA-QD conjugates resulted in the specific collection of QDs onto the corresponding Au patterns due to the specific interaction between the DNA-QD conjugate and the DNA-Au patterns. Although the authors' initial purpose was to sort the fluorescent nanocrystals, the resulting QD-coated Au patterns possessed the specific fluorescence emission, which is suitable for the multiplexed detection of biological targets at the nanometer scale.

Kim *et al.* have developed a novel biosensor for Hg^{2+} detection with a chip patterned by polydiacetylene (Figure 13) (151). The diacetylene molecules have an epoxy group that provides the versatile linkage chemistry for bioconjugation with biological molecules. The polydiacetylene-liposome microarray was obtained by the successive modification of glass substrate using amine functionality, amidation of epoxy liposomes, and linkage of

single strand DNA aptamer. The red-phase polydiacetylene emitted the fluorescence that was dependent on the external stimuli. After addition of Hg^{2+}, the formation of T-Hg^{2+}-T complexes caused the configuration change of the T-rich DNA aptamer, leading to the change in the fluorescence emission. This sensor exhibited a detection limit as low as 5 μM Hg^{2+}.

7. SUMMARY AND OUTLOOK

This review does not intend to cover the entire literature on the biosensors based on nanomaterials and nanostructures. Instead, it highlights the efficient enhancement of biosensor performance by the application of nanomaterials and nanostructures from several important aspects.

When nanomaterials or nanostructures are incorporated into biosensors, their unique physicochemical properties open up numerous possibilities for improvement of the sensing performance. The resulting new area of nano-bio-sensing sets a good example on the interaction among material sciences, physics, chemistry and biology at the nanoscale. The future outlook for this field is quite promising, because the unique physicochemical properties of nanomaterials and nanostructures that could not be accomplished by conventional bulk materials. From the recent representative publications being reviewed, it can be concluded that incorporation of biomolecules with nanomaterials/nanostructures to an integrated system is an effective way to construct biosensors with enhanced sensitivity and selectivity, faster response time, lower power consumption, and feasible miniaturization. In a word, we can expect more from the nanomaterial applications into biosensors. What is particularly noticeable is the emergence of graphene, a 2-D carbon-based nanomaterial, has opened a new horizon in the nano world.

It is worth noting that, different from the traditional separation between transducers and molecular recognition probes, a novel tactic is to integrate transducers with molecular recognition probes to form nano-transducers that recognize the binding events and actively transduce sensing signals simultaneously (152).

Most of past research on the nanostructured biosensors was the proof-of-concept work that demonstrated the advantages of nanomaterials and nanostructures. In the future, more efforts need to be made to move the proof-of-concept studies to the applications of biosensors to the real-world samples. One trend of future research is the integration of nanostructured sensors with microfluidics to form lab-on-chip devices. Furthermore, more studies need to be performed to integrate the nanostructured sensors with signal-processing instruments to build portable devices for on-site measurement of analytes to meet the need for on-time (real-time) monitoring the targets of interest and rapid assessment of risks. One of the resulting examples is the point-of-care device that has an increasing need in the commercial market.

8. ACKNOWLEDGEMENTS

This work was financially supported by the NSF grant (CBET-0834233) and NIH grant (1R43CA154339-01). The resource was partially supported by NSF (EPS 1003907), the West Virginia University Research Corporation and the West Virginia EPSCoR Office.

9. REFERENCES

1. J Wang: Nanomaterial-based electrochemical biosensors. *Analyst* 130, 421-426 (2005)

2. A Vaseashta, D Dimova-Malinovska: Nanostructured and nanoscale devices, sensors and detectors. *Sci Technol Adv Mat* 6, 312-318 (2005)

3. L Dyadyusha, H Yin, S Jaiswal, T Brown, JJ Baumberg, FP Booye, T Melvin: Quenching of CdSe quantum dot emission, a new approach for Biosensing. *Chem Commun,* 3201–3203 (2005)

4. J Liu, Y Lu: A colorimetric lead biosensor using DNAzyme-directed assembly of gold nanoparticles. *J Am Chem Soc 125*, 6642–6643 (2003)

5. A Neely, C Perry, B Varisli, AK Singh, T Arbneshi, D Senapati, JR Kalluri, PC Ray: Ultrasensitive and highly selective detection of alzheimer's disease biomarker using two-photon rayleigh scattering properties of gold nanoparticle. *ACS Nano* 3, 2834–2840 (2009)

6. L Hu, HS Kim, JY Lee, P Peumans, Y Cui: Scalable coating and properties of transparent, flexible, silver nanowire electrodes. *ACS Nano* 4, 2955–2963 (2010)

7. X Lu, MS Yavuz, HY Tuan, BA Korgel, Y Xia: Ultrathin gold nanowires can be obtained by reducing polymeric strands of oleylamine-AuCl complexes formed via aurophilic interaction. *J Am Chem Soc* 130, 8900–8901 (2008)

8. JK Jaiswal, H Mattoussi, JM Mauro, SMSimon: Long-term multiple color imaging of live cells using quantum dot bioconjugates. *Nat Biotechnol* 21, 47-51 (2003)

9. SA El-Safty, D Prabhakaran, Y Kiyozumi, F Mizukami: Nanoscale membrane strips for benign sensing of HgII Ions: a route to commercial waste treatments. *Adv Func Mater* 18, 1739–1750 (2008)

10. D Zhang, O Neumann, H Wang, VM Yuwono, A Barhoumi, M Perham, JD Hartgerink, P Wittung-Stafshede, NJ Halas: Gold nanoparticles can induce the formation of protein-based aggregates at physiological pH. *Nano Lett* 9, 666-671 (2009)

11. W Zhao, W Chiuman, JCF Lam, SA McManus, W Chen, Y Cui, R Pelton, MA Brook, Y Li: DNA aptamer folding on gold nanoparticles: from colloid chemistry to biosensors. *J Am Chem Soc* 130, 3610–3618 (2008)

12. AG Brolo, R Gordon, B Leathem, KL Kavanagh: Surface plasmon sensor based on the enhanced light transmission through arrays of nanoholes in gold films. *Langmuir* 20, 4813-4815 (2004)

13. L He, MD Musick, SR Nicewarner, FG Salinas, SJ Benkovic, MJ Natan, CD Keating: Colloidal Au-enhanced surface plasmon resonance for ultrasensitive detection of DNA hybridization. *J Am Chem Soc* 122, 9071-9077 (2000)

14. SJ Oldenburg, CC Genick, KA Clark, DA Schultzb: Base pair mismatch recognition using plasmon resonant particle labels. *Anal Biochem* 309, 109–116 (2002)

15. X Peng, MC Schlamp, AV Kadavanich, AP Alivisatos: Epitaxial growth of highly luminescent CdSe/CdS core/shell nanocrystals with photostability and electronic accessibility. *J Am Chem Soc* 119, 7019-7029 (1997)

16. J Elbaz, ZG Wang, R Orbach, I Willner: pH-stimulated concurrent mechanical activation of two DNA "tweezers". a "SET-RESET" logic gate system. *Nano Lett* 9, 4510–4514 (2009)

17. JA Malen, P Doak, K Baheti, TD Tilley, A Majumdar, RA Segalman: The nature of transport variations in molecular heterojunction electronics. *Nano Lett* 9, 3406–3412 (2009)

18. N Gaponik, SG Hickey, D Dorfs, AL Rogach, A Eychmüller: Progress in the light emission of colloidal semiconductor nanocrystals. *Small* 6, 1364–1378 (2010)

19. EM Nolan, SJ Lippard: Tools and tactics for the optical detection of mercuric Ion. *Chem Rev* 108, 3443–3480 (2008)

20. RC Somers, MG Bawendi, DG Nocera: CdSe nanocrystal based chem-/bio- sensors. *Chem Soc Rev* 36, 579–591 (2007)

21. DA Giljohann, DS. Seferos, WL Daniel, MD. Massich, PC. Patel, CA. Mirkin: Gold nanoparticles for biology and medicine. *Angew Chem Int Ed* 49, 3280–3294 (2010)

22. A Ramanavièius, FW Herberg, S Hutschenreiter, B Zimmermann, I Lapënaitë, A Kaušaitë, A Finkelšteinas, A Ramanavièienë: Biomedical application of surface plasmon resonance Biosensors. *Acta Medica Lituanica* 3, 1-9 (2005)

23. JP Camden, JA Dieringer, J Zhao, RP Van Duyne: Controlled plasmonic nanostructures for surface-enhanced spectroscopy and sensing. *Acc Chem Res* 41, 1653-1661 (2008)

24. J Hu, LS Li, W Yang, L Manna, LW Wang, AP Alivisatos: Linearly polarized emission from colloidal semiconductor quantum rods. *Science* 292, 2060-2063 (2001)

25. X Peng, L Manna, W Yang, J Wickham, E Scher, A Kadavanich, AP Alivisatos: Shape control of CdSe nanocrystals. *Nature* 404, 59-61 (2000)

26. K Kerman, M Saito, E Tamiya, S Yamamura, Y Takamura: Nanomaterial-based electrochemical biosensors for medical applications. *TrAC-Trend Anal Chem* 27, 585-592 (2008)

27. N Wu, M Zhao, JG Zheng, C Jiang, B Myers, S Li, M Chyu, SX Mao: Porous CuO-ZnO nanocomposite for sensing electrode of high-temperature CO solid-state electrochemical sensor. *Nanotechnology* 16, 2878-2881 (2005)

28. J Zang, CM Li, X Cui, J Wang, X Sun, H Dong, CQ Sun: Tailoring zinc oxide nanowires for high performance amperometric glucose sensor. *Electroanal* 19, 1008-1014 (2007)

29. J Yu, S Liu, H Ju**:** Glucose sensor for flow injection analysis of serum glucose based on immobilization of glucose oxidase in titania sol-gel membrane. *Biosens Bioelectron* 19, 401-409 (2003)

30. NQ Wu, H Li: One-dimensional nanostructures for chemical sensors and biosensors. in: handbook of nanoceramics and their based nanodevices. Eds: T.-Y. Tseng, H. S. Nalwa, *American Scientific Publishers*, Valencia, California (2009)

31. D Ivnitski, B Branch, P Atanassov, C Apblett: Glucose oxidase anode for biofuel cell based on direct electron transfer. *Electrochem Commun* 8, 1204-1210 (2006)

32. F Qu, M Yang, G Shen, R Yu: Electrochemical biosensing utilizing synergic action of carbon nanotubes and platinum nanowires prepared by template synthesis. *Biosens Bioelectron* 22, 1749-1755 (2007)

33. KB Male, S Hrapovic, Y Liu, D Wang, JHT Luong: Electrochemical detection of carbohydrates using copper nanoparticles and carbon nanotubes. *Anal Chim Acta* 516, 35-41 (2004)

34. W Yang, J Wang, S Zhao, Y Sun, C Sun: Multilayered construction of glucose oxidase and gold nanoparticles on Au electrodes based on layer-by-layer covalent attachment. *Electrochem Commun* 8, 665-672 (2006)

35. DR Thévenot, K Toth, RA Durst, GS Wilson: Electrochemical biosensors: Recommended definitions and classification - (Technical Report). *Pure Appl Chem* 71, 2333-2348 (1999)

36. M Yang, J Wang, H Li, JG Zheng, NN Wu: A lactate electrochemical biosensor with a titanate nanotube as direct electron transfer promoter. *Nanotechnology* 19, 075502 (2008)

37. E Topoglidis, AEG Cass, G Gilardi, S Sadeghi, N Beaumont, JR Durrant: Protein adsorption on nanocrystalline TiO2 films: An immobilization strategy for bioanalytical devices. *Anal Chem* 70, 5111-5113 (1998)

38. H Tokudome, M Miyauchi: Electrochromism of titanate-based nanotubes. *Angew Chem Int Ed* 44, 1974-1977 (2005)

39. F Caruso: Nanoengineering of particle surfaces. *Adv Mater* 13, 11-22 (2001)

40. CM Niemeyer: Nanoparticles, proteins, and nucleic acids: biotechnology meets materials science. *Angew Chem Int Ed* 40, 4128-4158 (2001)

41. E Katz, I Willner: Integrated nanoparticle-biomolecule hybrid systems: Synthesis, properties, and applications. *Angew Chem Int Ed* 43, 6042-6108 (2004)

42. R Cui, H Huang, Z Yin, D Gao, JJ Zhu: Horseradish peroxidase-functionalized gold nanoparticle label for amplified immunoanalysis based on gold nanoparticles/carbon nanotubes hybrids modified biosensor. *Biosens Bioelectron* 23, 1666-1673 (2008)

43. L Deng, Y Wang, L Shang, D W, F Wang, S Dong: A sensitive NADH and glucose biosensor tuned by visible light based on thionine bridged carbon nanotubes and gold nanoparticles multilayer. *Biosens Bioelectron* 24, 951-957 (2008)

44. R Li, X Cui, W Hu, Z Lu, CM Li**:** Fabrication of oriented poly-L-lysine/bacteriorhodopsin-embedded purple membrane multilayer structure for enhanced photoelectric response. *J Colloid Interf Sci* 344, 150-157 (2010)

45. D Chen, G Wang, J Li: Interfacial bioelectrochemistry: fabrication, properties and applications of functional nanostructured biointerfaces. *J Phys Chem C* 111, 2351-2367 (2006)

46. D Lee, T Cui : Layer-by-layer self-assembled single-walled carbon nanotubes based ion-sensitive conductometric glucose biosensors. IEEE Sens J 9, 449-456 (2009)

47. DWM Arrigan: Nanoelectrodes, nanoelectrode arrays and their applications. Analyst 129, 1157-1165 (2004)

48. AC Pereira, A Kisner, N Duran, LT Kubota: The effects of dimensionality on electrochemical sensors based on carbon nanotubes and metallic nanowires. J Nanosci Nanotechno 10, 651-667 (2010)

49. W Yantasee, K Hongsirikarn, CL Warner, D Choi, T Sangvanich, MB Toloczko, MG Warner, GE Fryxell, RS Addleman, C Timchalk: Direct detection of Pb in urine and Cd, Pb, Cu, and Ag in natural waters using electrochemical sensors immobilized with DMSA functionalized magnetic nanoparticles. *Analyst* 133, 348-355 (2008)

50. H Li, N Wu: A large-area nanoscale gold hemisphere pattern as a nanoelectrode array. *Nanotechnology* 19, 275301 (2008)

51. Y Yun, Z Dong, V Shanov, WR Heineman, HB Halsall, A Bhattacharya, L Conforti, RK Narayan, WS Ball, MJ Schulz: Nanotube electrodes and biosensors. *Nano Today* 2, 30-37 (2007)

52. AL Crumbliss, SC Perine, J Stonehuerner, KR Tubergen, JG Zhao, RW Henkens: Colloidal gold as a biocompatible immobilization matrix suitable for the fabrication of enzyme electrodes by electrodeposition. *Biotechnol Bioeng* 40, 483-490 (1992)

53. J Zhao, RW Henkens, J Stonehuerner, JP O'Daly, AL Crumbliss: Direct electron-transfer at horseradish-peroxidase colloidal gold modified electrodes. *J Electroanal Chem* 327, 109-119 (1992)

54. A Guiseppi-Elie, C Lei, RH Baughman: Direct electron transfer of glucose oxidase on carbon nanotubes. *Nanotechnology* 13, 559-564 (2002)

55. F Patolsky, Y Weizmann, I Willner: Long-range electrical contacting of redox enzymes by SWCNT connectors. *Angew Chem Int Ed* 43, 2113-2117 (2004)

56. Y Xiao, F Patolsky, E Katz, JF Hainfeld, I Willner: "Plugging into enzymes": nanowiring of redox enzymes by a gold nanoparticle. *Science* 299, 1877-1881 (2003)

57. RM Wightman: Voltammetry with microscopic electrodes in new domains. *Science* 240, 415-420 (1988)

58. RM Penner, MJ Heben, TL Longin, NS Lewis: Fabrication and use of nanometer-sized electrodes in electrochemistry, *Science* 250, 1118-1121 (1990)

59. S Hrapovic, JHT Luong: Picoamperometric Detection of glucose at ultrasmall platinum-based biosensors: preparation and characterization, *Anal Chem* 75, 3308-3315 (2003)

60. TJ Davies, SWJ, CE Banks, J del Campo, R Mas, FX Muñoz, RG Compton: The cyclic and linear sweep voltammetry of regular and random arrays of microdisc electrodes: Fitting of experimental data, *J Electroanal Chem* 585, 63-82 (2005)

61. LM Moretto, N Pepe, P Ugo: Voltammetry of redox analytes at trace concentrations with nanoelectrode ensembles, *Talanta* 62, 1055–1060 (2004)

62. VP Menon, CR Martin: Fabrication and evaluation of nanoelectrode ensembles, *Anal Chem* 67, 1920-1928 (1995)

63. P Ugo, LM Moretto, S Bellomi, VP Menon, CR Martin: Ion exchange voltammetry at polymer film coated nanoelectrode ensembles, *Anal Chem* 68, 4160-4165 (1996)

64. E Sabatani, I Rubinstein: Organized self-assembling monolayers on electrodes. 2. Monolayer-based ultramicroelectrodes for the study of very rapid electrode-kinetics. *J Phys Chem* 91, 6663-6669 (1987)

65. AM Bond, KB Oldham, CG Zoski: Steady-state voltammetry. *Anal Chim Acta* 216, 177-230 (1989)

66. J Li, HT Ng, A Cassell, W Fan, H Chen, QYe, J Koehne, J Han, M Meyyappan: Carbon nanotube

nanoelectrode array for ultrasensitive DNA detection. *Nano Lett* 3, 597-602 (2003)

67. CJ Murphy, AM Gole, SE Hunyadi, JW Stone, PN Sisco, A Alkilany, BE Kinard, P Hankins: Chemical sensing and imaging with metallic nanorods. *Chem Commun*, 544–557 (2008)

68. LS Live, O R Bolduc, J-F Masson: Propagating surface plasmon resonance on microhole arrays. *Anal Chem* 82, 3780–3787 (2010)

69. LM Liz-Marzán: Tailoring surface plasmons through the morphology and assembly of metal nanoparticles. *Langmuir* 22, 32-41 (2006)

70. SK Ghosh, T Pal: Interparticle coupling effect on the surface plasmon resonance of gold nanoparticles: from theory to applications. *Chem Rev* 107, 4797-4862 (2007)

71. AJ Haes, RP Van Duyne: A unified view of propagating and localized surface plasmon resonance biosensors. *Anal Bioanal Chem* 379, 920–930 (2004)

72. ECL Ru, PG Etchegoin: Principles of surface-enhanced Raman spectroscopy and related plasmonic effects. *Elsevier*, London (2009)

73. X Xu, WL Daniel, W Wei, CA Mirkin: Colorimetric Cu2+ detection using DNA-modified gold-nanoparticle aggregates as probes and click chemistry. *Small* 6, 623-626 (2010)

74. JM Slocik, JS Zabinski, Jr., DM Phillips, RR Naik: Colorimetric response of peptide-functionalized gold nanoparticles to metal ions. *Small* 4, 548–551 (2008)

75. Y Jiang, H Zhao, Y Lin, N Zhu, Y Ma, L Mao: Colorimetric detection of glucose in rat brain using gold nanoparticles. *Angew Chem Int Ed* 49, 4800–4804 (2010)

76. JR Kalluri, T Arbneshi, SA Khan, A Neely, P Candice, B Varisli, M Washington, S McAfee, B Robinson, S Banerjee, AK Singh, D Senapati, PC Ray: Use of gold nanoparticles in a simple colorimetric and ultrasensitive dynamic light scattering assay: selective detection of arsenic in groundwater. *Angew Chem Int Ed* 48, 9668 – 9671 (2009)

77. J Wang, HS Zhou: Aptamer-based Au nanoparticles-enhanced surface plasmon resonance detection of small molecules. *Anal Chem* 80, 7174–7178 (2008)

78. L Wu, HS Chu, WS Koh, EP Li: Highly sensitive graphene biosensors based on surface plasmon resonance. *Opt Express* 18, 14395-14400 (2010)

79. C Yu, J Irudayaraj: Multiplex biosensor using gold nanorods. *Anal Chem* 79, 572-579 (2007)

80. W Wang, H Cui: Chitosan-luminol reduced gold nanoflowers: from one-pot synthesis to morphology-dependent SPR and chemiluminescence sensing. *J Phys Chem C* 112, 10759–10766 (2008)

81. T Huang, F Meng, L Qi: Controlled synthesis of dendritic gold nanostructures assisted by supramolecular complexes of surfactant with cyclodextrin. *Langmuir* 26, 7582–7589 (2010)

82. Y Xiong, JM McLellan, J Chen, Y Yin, ZY Li, Y Xia: Kinetically controlled synthesis of triangular and hexagonal nanoplates of palladium and their SPR/SERS properties. *J Am Chem Soc* 127, 17118-17127 (2005)

83. X Zhang, RP Van Duyne: Optimized silver film over nanosphere surfaces for the biowarfare agent detection based on surface-enhanced Raman spectroscopy. *Mater Res Soc Symp Proc* 876E, R8.54.1-R8.54.6 (2005)

84. SM Marinakos, S Chen, A Chilkoti: Plasmonic detection of a model analyte in serum by a gold nanorod sensor. *Anal Chem* 79, 5278-5283 (2007)

85. PK Jain, W Huang, MA El-Sayed: On the universal scaling behavior of the distance decay of plasmon coupling in metal nanoparticle pairs: A Plasmon Ruler Equation. *Nano Lett* 7, 2080-2088 (2007)

86. JC Riboh, AJ Haes, AD McFarland, CR Yonzon, RP Van Duyne: A nanoscale optical biosensor: real-time immunoassay in physiological buffer enabled by improved nanoparticle adhesion. *J Phys Chem B* 107, 1772-1780 (2003)

87. M Fleischmann, PJ Hendra, AJ McQuillan: Raman spectra of pyridine adsorbed at a silver electrode. *Chem Phys Lett* 26, 163-166 (1974)

88. BNJ Persson, K Zhao, Z Zhang: Chemical contribution to surface-enhanced Raman scattering. *Phys Rev Lett* 96, 207401 (2006)

89. H Xu, J Aizpurua, M Käll, P Apell: Electromagnetic contributions to single-molecule sensitivity in surface-enhanced Raman scattering. *Phys Rev E* 62, 4318-4324 (2000)

90. SM Morton, L Jensen: Understanding the molecule-surface chemical coupling in SERS. *J Am Chem Soc* 131, 4090–4098 (2009)

91. S Nie, SR Emory: Probing single molecules and single nanoparticles by surface-enhanced Raman scattering. *Science* 275, 1102-1106 (1997)

92. DK Lim, KS Jeon, HM Kim, JM Nam, YD Suh: Nanogap-engineerable Raman-active nanodumbbells for single-molecule detection. *Nat Mater* 9, 60-67 (2010)

93. SSR Dasary, AK Singh, D Senapati, H Yu, PC Ray: Gold Nanoparticle based label-free SERS probe for ultrasensitive and selective detection of trinitrotoluene. *J Am Chem Soc* 131, 13806–13812 (2009)

94. WE Doering, ME Piotti, MJ Natan, RG Freeman: SERS as a foundation for nanoscale, optically detected biological labels. *Adv Mater* 19, 3100–3108 (2007)

95. G Braun, SJ Lee, M Dante, TQ Nguyen, M Moskovits, N Reich: Surface-enhanced Raman spectroscopy for DNA detection by nanoparticle assembly onto smooth metal films. *J Am Chem Soc* 129, 6378-6379 (2007)

96. CJ Orendorff, A Gole, TK Sau, CJ Murphy: Surface-enhanced Raman spectroscopy of self-assembled monolayers: sandwich architecture and nanoparticle shape dependence. *Anal Chem* 77, 3261-3266 (2005)

97. M Sanles-Sobrido, W Exner, L Rodríguez-Lorenzo, B Rodríguez-González, MA Correa-Duarte, RA Álvarez-Puebla, LM Liz-Marzán: Design of SERS-encoded, submicron, hollow particles through confined growth of encapsulated metal nanoparticles. *J Am Chem Soc* 131, 2009, 2699–2705

98. JB Jackson, NJ Halas: Surface-enhanced Raman scattering on tunable plasmonic nanoparticle substrates. *PNAS* 101, 17930-17935 (2004)

99. W Li, PHC Camargo, X Lu, Y Xia: Dimers of silver nanospheres: facile synthesis and their use as hot spots for surface-enhanced Raman scattering. *Nano Lett* 9, 485–490 (2009)

100. G Chen, Y Wang, M Yang, J Xu, SJ Goh, M Pan, H Chen: Measuring ensemble-averaged surface-enhanced Raman scattering in the hotspots of colloidal nanoparticle dimers and trimers. communication measuring ensemble-averaged surface-enhanced Raman scattering in the hotspots of colloidal nanoparticle dimers and trimers. *J Am Chem Soc* 132, 3644–3645 (2010)

101. SEJ Bell, NMS Sirimuthu: Surface-enhanced Raman spectroscopy (SERS) for sub-micromolar detection of DNA/RNA mononucleotides. *J Am Chem Soc* 128, 15580-15581 (2006)

102. T Kang, SM Yoo, I Yoon, SY Lee, B Kim: Patterned multiplex pathogen DNA detection by Au particle-on-wire SERS sensor. *Nano Lett* 10, 1189-1193 (2010)

103. T Kang, I Yoon, KS Jeon, W Choi, Y Lee, K Seo, Y Yoo, QH Park, H Ihee, YD Suh, B Kim: Creating well-defined hot spots for surface-enhanced Raman scattering by single-crystalline noble metal nanowire pairs. *J Phys Chem C* 113, 7492–7496 (2009)

104. PHC Camargo, M Rycenga, L Au, Y Xia: Isolating and probing the hot spot formed between two silver nanocubes. *Angew Chem Int Ed* 48, 2180 –2184 (2009)

105. BK Jena, CR Ra: Seedless, Surfactantless room temperature synthesis of single crystalline fluorescent gold nanoflowers with pronounced SERS and electrocatalytic activity. *Chem Mater* 20, 3546–3548 (2008)

106. Q Zhou, Y Chao, Y Li, W Xu, Y Wu, J Zheng: Contribution of Charge-Transfer Mechanisms to Surface-Enhanced Raman Scattering with Near-IR Excitation. *ChemPhysChem* 8, 921-925 (2007)

107. WE Doering, S Nie: Spectroscopic Tags using dye-embedded nanoparticles and surface-enhanced Raman scattering. *Anal Chem* 75, 6171-6176 (2003)

108. JF Li, YF Huang, Y Ding, ZL Yang, SB Li, XS Zhou, FR Fan, W Zhang, ZY Zhou, DY Wu, B Ren, ZL Wang, ZQ Tian: Shell-isolated nanoparticle-enhanced Raman Spectroscopy. *Nature* 464, 392-395 (2010)

109. YWC Cao, R Jin, CA Mirkin: Nanoparticles with Raman spectroscopic fingerprints for DNA and RNA detection. *Science* 297, 1536-1539 (2002)

110. P Zhang, Y Guo: Surface-enhanced Raman scattering inside metal nanoshells. *J Am Chem Soc* 131, 3808–3809 (2009)

111. X Zhang, MA Young, O Lyandres, RP Van Duyne: Rapid detection of an anthrax biomarker by surface-enhanced Raman spectroscopy. *J Am Chem Soc* 127, 4484-4489 (2005)

112. AJ Haes, CL Haynes, AD McFarland, GC Schatz, RP Van Duyne, S Zou: Plasmonic materials for surface-enhanced sensing and spectroscopy. *MRS Bull* 30, 368-375 (2005)

113. Q Yu, P Guan, D Qin, G Golden, PM Wallace: Inverted size-dependence of surface-enhanced Raman scattering on gold nanohole and nanodisk Arrays. *Nano Lett* 8, 1923-1928 (2008)

114. Y Chu, MG Banaee, KB Crozier: Double-resonance plasmon substrates for surface-enhanced Raman scattering with enhancement at excitation and stokes frequencies. *ACS Nano* 4, 2804-2810 (2010)

115. MG Banaee, KB Crozier: Gold nanorings as substrates for surface-enhanced Raman scattering. *Opt Lett* 35, 760-762 (2010)

116. Y Chu, KB Crozier: Experimental study of the interaction between localized and propagating surface plasmons. *Opt Lett* 34, 244-246 (2009)

117. L Fabris, M Schierhorn, M Moskovits, GC Bazan: Aptatag-based multiplexed assay for protein detection by surface-enhanced Raman spectroscopy. S*mall* 14, 1550–1557 (2010)

118. M Hagihara, M Fukuda, T Hasegawa, T Morii: A modular strategy for tailoring fluorescent biosensors from ribonucleopeptide complexes. *J Am Chem Soc* 128, 12932-12940 (2006)

119. A Sassolas, BD Leca-Bouvier, LJ Blum: DNA biosensors and microarrays. *Chem Rev* 108, 109-139 (2008)

120. M Bruchez Jr, M Moronne, P Gin, S Weiss, AP Alivisatos: Semiconductor nanocrystals as fluorescent biological labels. *Science* 281, 2013-2016 (1998)

121. IL Medintz, AR Clapp, H Mattoussi, ER Goldman, B Fisher, JM Mauro: Self-assembled nanoscale biosensors based on quantum dot FRET donors. *Nat Mater* 2, 630-638 (2003)

122. WCW Chan, S Nie: Quantum dot bioconjugates for ultrasensitive nonisotopic detection. *Science* 281, 2016-2018 (1998)

123. DS Lidke, P Nagy, R Heintzmann, DJ Arndt-Jovin, JN Post, HE Grecco, EA Jares-Erijman, TM Jovin: Quantum dot ligands provide new insights into erbB/HER receptor–mediated signal transduction. *Nat Biotechnol* 22, 198-203 (2004)

124. R Freeman, T Finder, L Bahshi, I Willner: β-Cyclodextrin-modified CdSe/ZnS quantum dots for sensing and chiroselective analysis. *Nano Lett* 9, 2073–2076 (2009)

125. W Cai, DW Shin, K Chen, O Gheysens, Q Cao, SX Wang, SS Gambhir, X Chen: Peptide-labeled near-infrared quantum dots for imaging tumor vasculature in living subjects. *Nano Lett* 6, 669-676 (2006)

126. D Geiβer, LJ Charbonnière, RF Ziessel, NG Butlin, HG Löhmannsröben, N Hildebrandt: Quantum dot biosensors for ultrasensitive multiplexed diagnostics. *Angew Chem Int Ed* 49, 1-6 (2010)

127. K Susumu, HT Uyeda, IL Medintz, T Pons, JB Delehanty, H Mattoussi: Enhancing the stability and biological functionalities of quantum dots via compact multifunctional ligands. *J Am Chem Soc* 129, 13987-13996 (2007)

128. SK Dixit, NL Goicochea, MC Daniel, A Murali, L Bronstein, M De, B Stein, VM. Rotello, CC Kao, B Dragnea: quantum dot encapsulation in viral capsids. *Nano Lett* 6, 1993-1999 (2006)

129. W Jiang, S Mardyani, H Fischer, WCW Chan: Design and characterization of lysine cross-linked mercapto-acid biocompatible quantum dots. *Chem Mater* 18, 872-878 *(*2006)

130. AM Dennis, G Bao: Quantum dot-fluorescent protein pairs as novel fluorescence resonance energy transfer probes. *Nano Lett* 8, 1439–1445 (2008)

131. R Roy, S Hohng, T Ha: A practical guide to single-molecule FRET. *Nat Method* 5, 507-516 (2008)

132. AR Clapp, IL Medintz, JM Mauro, BR Fisher, MG Bawendi, H Mattoussi: Fluorescence resonance energy transfer between quantum dot donors and dye-labeled protein acceptors. *J Am Chem Soc* 126, 301-310 (2004)

133. ER Goldman, IL Medintz, JL Whitley, A Hayhurst, AR Clapp, HT Uyeda, JR Deschamps, ME Lassman, H Mattoussi: A hybrid quantum dot-antibody fragment fluorescence resonance energy transfer-based TNT sensor. *J Am Chem Soc* 127, 6744-6751 (2005)

134. R Gill, I Willner, I Shweky, U Banin: Fluorescence resonance energy transfer in CdSe/ZnS-DNA conjugates: probing hybridization and DNA cleavage. *J Phys Chem B* 109, 23715-23719 (2005)

135. DJ Maxwell, JR Taylor, S Nie: Self-assembled nanoparticle probes for recognition and detection of biomolecules. *J Am Chem Soc* 124, 9606-9612 (2002)

136. TL Jennings, MP Singh, GF Strouse: Fluorescent lifetime quenching near d =1.5 nm gold Nanoparticles: probing NSET validity. *J Am Chem Soc* 128, 5462-5467 (2006)

137. T Pons, IL Medintz, KE Sapsford, S Higashiya, AF Grimes, DS English, H Mattoussi: On the quenching of semiconductor quantum dot photoluminescence by proximal gold nanoparticles. *Nano Lett* 7, 3157-3164 (2007)

138. M Kondon, J Kim, N Udawatte, D Lee: Origin of size-dependent energy transfer from photoexcited CdSe quantum dots to gold nanoparticles. *J Phys Chem C* 112*,* 6695-6699 (2008)

139. RC Stringera, S Schommerb, D Hoehna, SA Grant: Development of an optical biosensor using gold nanoparticles and quantum dots for the detection of porcine reproductive and respiratory syndrome virus*. Sensor Actuat B: Chem* 134, 427–431 (2008)

140. CC Huang, Z Yang, KH Lee, HT Chang: Synthesis of highly fluorescent gold nanoparticles for sensing mercury (II). *Angew Chem Int Ed* 46, 6824 –6828 (2007)

141. L Shang, Sh Dong: Sensitive detection of cysteine based on fluorescent silver clusters. *Biosens Bioelectro* 24, 1569–1573 (2009)

142. S Huang, Y Chen: Ultrasensitive fluorescence detection of single protein molecules manipulated electrically on Au nanowire. *Nano Lett* 8, 2829–2833 (2008)

143. JH Jung, DS Cheon, F Liu, KB Lee, TS Seo: A graphene oxide based immuno-biosensor for pathogen detection. *Angew Chem Int Ed* 49, 1–5 (2010)

144. R Yang, J Jin, Y Chen, N Shao, H Kang, Z Xiao, Z Tang, Y Wu, Z Zhu, W Tan: Carbon nanotube-quenched fluorescent oligonucleotides: probes that fluoresce upon hybridization. *J Am Chem Soc* 130, 8351–8358 (2008)

145. J Li, XW Zhao, YJ Zhao, ZZ Gu: Quantum-dot-coated encoded silica colloidal crystals beads for multiplex coding. *Chem Commun,* 2329–2331 (2009)

146. SV Vaidya, ML Gilchrist, C Maldarelli, A Couzis: Spectral bar coding of polystyrene microbeads using multicolored quantum dots. *Anal Chem* 79, 8520-8530 (2007)

147. A Sukhanova, AS Susha, A Bek, S Mayilo, AL Rogach, J Feldmann, V Oleinikov, B Reveil, B Donvito, JHM Cohen, I Nabiev: Nanocrystal-encoded fluorescent microbeads for proteomics: antibody profiling and diagnostics of autoimmune diseases. *Nano Lett* 7, 2322-2327 (2007)

148. M Han, X Gao, JZ Su, S Nie: Quantum-dot-tagged microbeads for multiplexed optical coding of biomolecules. *Nat Biotechnol* 19, 631-635 (2001)

149. Z Li, Y Zhang, S Jiang: Multicolor core/shell-structured upconversion fluorescent nanoparticles. *Adv Mater* 20, 1–5 (2008)

150. D Gerion, WJ Parak, SC Williams, D Zanchet, CM Micheel, AP Alivisatos: Sorting fluorescent nanocrystals with DNA. *J Am Chem Soc* 124, 7070-7074 (2002)

151. J Lee, H Jun, J Kim: Polydiacetylene-liposome microarrays for selective and sensitive mercury (II) detection. *Adv Mater* 21, 3674–3677 (2009)

152. D Grieshaber, R MacKenzie, J Vörös, E Reimhult: Electrochemical biosensors-sensor principles and architectures. *Sensors* 8, 1400-1458 (2008)

Abbreviations: AA: ascorbic acid, CFU: colony forming unit, CM: Chemical enhancement, CNTs: carbon nanotubes, DHLA: dihydrolipoic acid , DMSA: dimercaptosuccinic acid , EM: electromagetic enhancement, FON: film over nanosphere , FRET: Förster resonance energy transfer, GCE: glassy carbon electrode, GNPs: gold nanoparticles, GOx: glucose oxidase, HS-PEG-COOH: HS-poly (ethylene glycol)-carboxyl acid, LBL: layer-by-layer, LOx: lactate oxidase, MPA: mercaptobenzoic acid, MWCNTs: multi-walled carbon nanotubes, NEAs: nanoelectrode arrays , NEEs: nanoelectrode ensembles, NPs: nanoparticles, NS: Nanosphere , NT: Nanotube , NW: Nanowire , PDDA: poly (diallyldimethylammonium chloride, PRRSV: Porcine Reproductive and Respiratory Syndrome Virus, PPY: polypyrrole , QDs: quantum dots, SERS: surface-enhanced Raman scattering, SPR: surface plasmon resonance, SWCNTs: single-walled carbon nanotubes, TNT: titanate nanotube or 2,4,6-trinitrotoluene, UA: uric acid

Key Words: Biosensors, SPR, SERS, Fluorescence, Electrochemistry, Review

Send correspondence to: Nianqiang Wu, Department of Mechanical and Aerospace Engineering, WVNano Initiative, West Virginia University, Morgantown, WV 26506-6106, USA, Tel: 304-293-3326, Fax: 304-293-6689, E-mail: nick.wu@mail.wvu.edu

http://www.bioscience.org/current/vol3S.htm